The inhibitory mechanism of a small protein reveals its role in antimicrobial peptide sensing

Shan Jiang[1], Lydia C. Steup[1], Charlotte Kippnich[1], Symela Lazaridi[2,3], Gabriele Malengo[1], Thomas Lemmin[2] and Jing Yuan[1]*

Abstract

A large number of small membrane proteins have been discovered in bacteria, but their mechanism of action has remained mostly elusive. Here, we investigate the mechanism of a physiologically important small protein, MgrB, which represses the activity of the sensor kinase PhoQ and is widely distributed among enterobacteria. The PhoQ/PhoP two-component system is a master regulator of the bacterial virulence program and interacts with MgrB to modulate bacterial virulence, fitness, and drug resistance. A combination of crosslinking approaches with functional assays and protein dynamic simulations revealed structural rearrangements due to interactions between MgrB and PhoQ near the membrane/periplasm interface and along the transmembrane helices. These interactions induce the movement of the PhoQ catalytic domain and the repression of its activity. Without MgrB, PhoQ appears to be much less sensitive to antimicrobial peptides, including the commonly used C18G. In the presence of MgrB, C18G promotes MgrB to dissociate from PhoQ, thus activating PhoQ via derepression. Our findings reveal the inhibitory mechanism of the small protein MgrB and uncover its importance in antimicrobial peptide sensing.

Significance Statement

Small proteins have high prevalence, vast diversity, and primarily regulatory functions in biological processes across all domains of life. However, their mechanisms of action remain largely elusive. In this study, we investigate the mechanism of the small protein, MgrB. It interacts with the sensor kinase PhoQ, rearranges its conformation, represses its kinase activity, and regulates bacterial response to environmental changes. In particular for antimicrobial peptides, MgrB is required for bacteria to have a selective response to this host-exclusive stimulus. Our findings underline the importance of a small protein in bacterial fitness and drug resistance and provide a molecular basis for engineering novel peptide-based regulators.

Introduction

Small proteins are defined by their short sequences (usually < 50 aa) and their direct synthesis via ribosomal translation. An increasing number of small proteins have been identified in individual species in all domains of life and complex biological communities, suggesting a high prevalence and vast diversity in biological systems (reviewed in [1-4]). Many of these small proteins (~30%) are located in the cell membrane or have been predicted to be located there (e.g., [5, 6]). Although only a few detailed studies of small membrane proteins have been conducted, results show that small proteins may target larger proteins and the lipid bilayer, regulating protein function, abundance, and changing membrane properties, demonstrating their predominant role as regulators in the lipid bilayer (reviewed in [7]).

The membrane located PhoQ sensor kinase, a master regulator of a bacterial virulence program, detects host-associated stimuli (review in [8]), such as cationic antimicrobial peptides (CAMPs) [9], mild acidic pH [10, 11], increased osmolarity [12], biliary unsaturated long-chain fatty acids [13], and magnesium limitation [14]. Three small membrane proteins have been identified to control PhoQ activity via direct protein-protein interactions. In *E. coli,* MgrB (47aa) and SafA (65aa) modulate PhoQ activity, with MgrB acting as an inhibitor and SafA as an activator [15,

16]. Deletion of *mgrB* or *safA* has physiological consequences, resulting in a cell division block under magnesium starvation or lowered acid resistance, respectively [17, 18]. In *Salmonella enterica* serovar Typhimurium, a species-specific small protein, UgtS (34 aa), was discovered recently and shown to control the timing of virulence gene expression by preventing premature PhoQ activation when inside macrophages [19].

The PhoQ sensor kinase is found as a dimer on the bacterial inner membrane. It consists of a periplasmic, a transmembrane (TM), a HAMP, a DHp, and a catalytic-ATP binding domain. In the periplasmic domain, several molecular interactions are essential for the functional state of the PhoQ molecule. These include the central hydrogen bonding network (T48 D179 K186) in the PAS-fold [20-23], the inter-monomeric salt bridge (D179-R50') [24], the membrane-facing acidic cluster (^{148}EDDDDAE) and the juxta-membrane region at the periplasm/inner-membrane interface [9, 23, 25]. Mutations altering these molecular interactions change the conformation of the periplasmic domain and the sensitivity of PhoQ to magnesium, low pH, and/or CAMPs. Additionally, different stimuli may result in distinct conformational states of the periplasmic domain, at least in an *in vitro* setting. For example, the PhoQ periplasmic domain showed divergent NMR spectra in low pH compared to that in low magnesium conditions [10]. Besides the periplasmic domain, the PhoQ transmembrane domain was shown to detect environmental osmotic upshifts, where the transmembrane four-helix bundle adopts a more compact and kinase-active conformation [12].

Among the known PhoQ-regulating small proteins, MgrB is the most widely distributed PhoQ repressor in enterobacteria. In *Salmonella*, the deletion of *mgrB* was shown to affect its infection of macrophages and epithelial cells [26]. In *Klebsiella pneumonia*, the disruption of the *mgrB* gene is the most prevalent among other chromosomal mutations in colistin-resistant strains [27]. The expression of *mgrB* is PhoPQ dependent. Thus, the inhibitory function of MgrB provides negative feedback to the two-component system resulting in a partial adaptation of *E. coli* to environmental changes [15, 28]. MgrB is a bitopic inner membrane protein with a short cytosolic N-terminus and a periplasmic C-terminal region (Fig. 1A). Two conserved cysteines (C28 and C39) in the periplasmic region were shown to be essential for MgrB function and suggested to form a disulfide bond [15]. This disulfide bond was proposed to allow MgrB to act as a sensor for the redox state of the bacterial periplasm and create an entry point for redox sensing by the PhoQ/PhoP system [29]. Besides the two cysteines, eight functionally essential residues were identified spread across the entire molecule [30]. However, the mechanism of MgrB inhibiting PhoQ remained largely unclear.

In this study, we combined crosslinking approaches with functional assays and protein dynamic simulations to identify interactions between PhoQ and MgrB, probe MgrB-induced PhoQ conformational changes, and examine the impact of MgrB on PhoQ sensing environmental stimuli. We propose that the binding of MgrB (i) changes the conformation of the linker region between PhoQ periplasmic and transmembrane domains, (ii) rearranges the transmembrane four-helix bundle, and (iii) initiates the translocation of the catalytic domain. MgrB interferes with PhoQ signaling, resulting in an overall lowered activity but still allows PhoQ activation under low pH, osmotic upshift, and magnesium limitation. We further reveal that MgrB mediates PhoQ sensing antimicrobial peptides, enabling bacteria to have a selective response to this exclusively host-associated stimulus.

Results

Structural predictions by Alphafold2

We used Alphafold2 multimer [31-33] to predict the structures of the PhoQ/MgrB complex as well as the individual component of the complex (Fig. 1B, C, and S1). The overall prediction of structural elements agrees with previous experimental evidence. For example, the two conserved periplasmic cysteine residues (C28 and C39) in MgrB were positioned in close proximity in the models, structurally supporting the presence of a disulfide bond. In the PhoQ predictions, the PAS fold in the periplasmic domain, the HAMP, the DHp, and the cytosolic catalytic-ATP binding domains resembled the experimental results of these structural motifs [24, 34]. Notably, the region connecting the periplasmic and TM domains and that connecting the HAMP and DHp domains showed a lower predicted local distance difference test loss (pLDDT) score (colored in yellow to green in Fig. S1), indicating these linker regions might have a higher capability of adopting different conformations. Unlike the asymmetric crystal structure of the PhoQ sensor domain [24], the Alphafold2 predicted PhoQ dimer was symmetric, which likely represented only one of many conformations that PhoQ could adopt. In all five PhoQ/MgrB complex models (Fig. 1B and S1), MgrB was placed in between the two PhoQ protomers, with the transmembrane helix parallel to the PhoQ TM helices and the C-terminal short helix (A40-W47) protruding away from PhoQ. The five predicted complex models had only minor differences regarding the positioning of MgrB. Because the PhoQ dimer was mostly symmetrical, Alphafold2 randomly placed MgrB on one or the other side of the PhoQ dimer (Fig. S1). When bound to PhoQ, MgrB showed a major conformational change in the region flanked by the two conserved cysteines (C28 and C39). This region had reduced helicity and rigidness, appearing as an extended flexible loop (Fig. 1C).

Disulfide crosslinking between MgrB and PhoQ TM helices

Before Alphafold was available, we used the disulfide crosslinking approach to identify the interacting residues in PhoQ and MgrB. We started with residue W20 in the MgrB TM helix, which was suggested to have direct contact with PhoQ [30]. Sequence alignment of MgrB homologs from different bacterial species revealed both W and Y conserved at position 20 (Fig. S2). The MgrB W20Y variant also showed strong inhibitory activity comparable to the wild type (Fig. S2). Since both W and Y have an aromatic ring structure and a polar moiety, we predicted that the nature of the interactions at position 20 likely include hydrophobic interactions and hydrogen bonding. Scanning through the sequence of the two PhoQ transmembrane helices, Y32 in TM1 appeared to be the optimal candidate to fulfill both types of interaction with MgrB W20.

To test this prediction with disulfide crosslinking, we constructed a PhoQ TM_Cys library and generated the MgrB C16A W20C variant, which has only one cysteine residue in the transmembrane helix. The Cys to Ala mutation at MgrB position 16 did not appear to have a functional effect (Fig. S2B). However, the Trp to Cys mutation at position 20 significantly reduced MgrB activity (Fig. S2A). To compensate for the loss of function, we increased the induction of MgrB C16A W20C (pTrc promoter with 10 μM IPTG), which ensured significant repression of PhoQ during crosslinking (Fig. S2D). Additionally, a FLAG tag was fused to the N-terminus of MgrB (Fig. S2E) to facilitate the detection of the PhoQ/MgrB complex in Western blot. Cu-phenanthroline was added to the cells to catalyze the disulfide formation between sulfhydryl groups at a close distance. When MgrB C16A W20C was co-expressed with PhoQ Y32C, we observed a higher molecular weight band at around 55 kDa on the Western blot

145 corresponding to the PhoQ/MgrB complex (Fig. 1D, S3A). This band was reduced by the addition
146 of dithiothreitol (DTT) and was absent when the cysteine residue was at position 16 (WT), or no
147 cysteine was in the MgrB transmembrane helix (C16A). The results are consistent with our
148 prediction suggesting the close proximity of MgrB W20 with the PhoQ TM1 residue Y32 in the
149 complex. Additionally, we found that PhoQ L204C crosslinked with MgrB W20C, indicating
150 position 20 near L204 in PhoQ TM2 as well (Fig. 1D, S3A). Furthermore, we tested PhoQ Cys
151 variants in the neighboring positions of 32 and 204 (PhoQ 31C, 33C, 203C, and 205C). None of
152 the variants formed detectable crosslinked complexes with MgrB W20C in the Western blot (Fig.
153 S2G). Functionally, both PhoQ Y32C and L204C mutants partially restored the MgrB inhibition
154 (Fig. S2F), supporting the hypothesis that MgrB W20 interacts with residue Y32 in PhoQ TM1
155 and L204 in PhoQ TM2.
156
157 Using MgrB residue 20 as a reference point, we next identified interacting amino acids of two
158 more functionally important residues (Q22 and F24) in the MgrB TM helix [30]. In both cases, we
159 observed stronger crosslinking bands and more than one crosslinked position in both
160 transmembrane helices of PhoQ (Fig. 1E, F, S3B, C). For MgrB Q22C, stronger crosslinks were
161 observed to residues in the PhoQ TM2 helix (colored blue). The strongest crosslinking band was
162 shown when PhoQ Y197C was co-expressed. The crosslinking efficiency decreased when the
163 cysteine residue moved to the neighboring positions and further away (196C, 195C, and 198C).
164 It was then partially recovered when the cysteine (194C) was roughly one helical turn away from
165 Y197 (Fig. 1E). Functionally, the Y197C mutation in PhoQ restored the MgrB Q22C activity the
166 best when compared to other PhoQ TM_Cys mutants, supporting the notion that MgrB Q22
167 primarily interacts with PhoQ Y197.
168
169 For MgrB F24C (Fig. 1F, S3C), the strongest crosslinking was found with a PhoQ TM1 mutant,
170 I38C. Functionally, PhoQ I38C showed the highest extent of activity reduction when co-
171 expressed with MgrB F24C, thus restoring the activity of MgrB F24C the best among the tested
172 PhoQ/MgrB pairs. The minor crosslinking events observed could be due to the greater distance
173 between the cysteine residues or an indication of intermediate binding states of MgrB. Notably,
174 one PhoQ Cys variant, F195C, retained only about 1% of the wild-type activity (Fig. 1E). Mutants
175 with such a severe functional defect may have altered MgrB binding, thus unsuitable for the
176 crosslinking approach. For other PhoQ variants in Fig. 1E and F, some showed moderately
177 reduced activity, possibly due to the reduced protein expression level (i.e., PhoQ W192C in Fig.
178 S3F). More importantly, the presence of MgrB significantly repressed the activity of these PhoQ
179 variants, indicating that the change caused by cysteine substitutions does not have a major
180 impact on MgrB inhibition.
181
182 Collectively, we identified four-pair residues of MgrB and PhoQ located in close proximity at the
183 protein interface of the complex: W20-Y32, W20-L204, Q22-Y197, and F24-I38. In the
184 AlphaFold2 predicted complex models, these crosslinked pairs were positioned less than 14 Å in
185 the top four ranked models (Table 1). Furthermore, Q22-Y197 and F24-I38 had shorter Cα - Cα
186 distances than the W20-Y32 and W20-L204 pairs, consistent with our experimental results that
187 the former two pairs showed higher crosslinking efficiency.
188
189 **Crosslinking in the periplasmic domains of PhoQ and MgrB**
190 To gain insights into PhoQ/MgrB interactions at the periplasmic domains, we attempted to
191 identify interacting residue pairs using site-specific photo-crosslinking [35]. We introduced an
192 amber stop codon at each residue in the MgrB periplasmic region (residues 25 to 47). The

193 photo-crosslinking amino acid, *p*-benzoyl-l-phenylalanine (*p*Bpa), was then incorporated into the
194 flag-tagged MgrB at the amber stop codon via the orthogonal $tRNA^{Amber}$ and the aminoacyl-tRNA
195 synthetase in *E. coli*. After UV irradiation, we detected bands with a molecular weight of ~55
196 kDa by anti-FLAG antibody when *p*Bpa was incorporated at positions 26, 30, 32, and 38,
197 indicating the formation of the UV-dependent crosslinked PhoQ/MgrB complex (Fig. 2A, S4).
198
199 The crosslinked products from positions 30, 32, and 38 could be purified and subjected to mass
200 spectrometry (MS) analysis (Fig. S4 and File S1). PhoQ was detected in all samples as the most
201 prominent protein. Only a small number of other proteins were identified, indicating the protein
202 purification steps were highly effective. MgrB was challenging to detect due to its small size,
203 high hydrophobicity, and a low number of potential MS-detectable peptides. However, we
204 increased the sample injection amount, which allowed for the successful identification of MgrB
205 in crosslinked complex samples, except when *p*Bpa was incorporated at position 38. This was
206 most likely due to the interference of the digestion step with the incorporated *p*Bpa. Despite the
207 successful identification of both PhoQ and MgrB in the crosslinked samples, confident MS
208 identification of MgrB-PhoQ crosslinked peptides providing clear evidence towards positioning
209 the two proteins in the complex was not possible. The lack of crosslinked products with other
210 *mgrB_amber* constructs (Fig. S4) could be due to the low efficiency of *p*Bpa incorporation (i.e.,
211 position 29) and/or the obstruction of the bulky unnatural amino acid on the binding of MgrB to
212 PhoQ. Most of the residues that resulted in crosslinked products were within the MgrB C28-C39
213 loop region, suggesting its possible direct interaction with PhoQ.
214
215 In the Alphafold2 complex model, the MgrB C28-C39 loop was close to the PhoQ linker region
216 connecting the periplasmic and the TM domains. To test whether the MgrB C28-C39 loop
217 interacts directly with the linker region, we performed disulfide crosslinking with MgrB D31C
218 and PhoQ_linker_Cys variants. Because of two essential cysteines in the MgrB periplasmic
219 region, we first tested if introducing a third cysteine would affect MgrB function. We observed
220 that the introduction of a third cysteine at position 31 did not reduce MgrB inhibition as much
221 as the single cysteine variant, C39A (Fig. S5), suggesting that the cysteine at position 31 does not
222 severely interfere with the C28-C39 disulfide bond formation. Therefore, MgrB D31C is suitable
223 for crosslinking experiments. The crosslinking results showed that MgrB 31C formed disulfide
224 linkages with cysteines in several positions in the PhoQ linker region (184-188) with a similar
225 amount of crosslinked complex (Fig. 2B, S3D). No crosslinked products were detectable in the
226 control sample, where the wild-type MgrB (C28 and C39) was co-expressed with
227 PhoQ_linker_Cys mutants (Fig. 2B, S3E). Our data thus support that MgrB D31 interacts with the
228 PhoQ linker region. The comparable amount of crosslinked complex at multiple positions is
229 probably due to the flexible nature of the MgrB C28-C39 loop.
230
231 **The conformational change of PhoQ linker region upon MgrB binding**
232 After mapping the MgrB binding site on PhoQ, we next sought to detect MgrB-induced PhoQ
233 conformational change by comparing the PhoQ dimer crosslinking pattern with MgrB to the one
234 without MgrB. For the PhoQ linker region, we focused on residues 187 and 188, which showed
235 different conformations in PhoQ monomer and dimer models (Fig. S6A). These two residues
236 were located at the periplasmic end of the TM2 helix and at a similar lateral position as the TM1
237 residue 43 (Fig. S6B). By monitoring the crosslinking efficiency between residues at positions 43
238 and 188, we intended to detect local helical movements upon MgrB binding. In the absence of
239 MgrB, we observed that 43C and 188C formed an intramolecular disulfide linkage, manifesting
240 as a faster-migrating band below the PhoQ monomer band (Fig. 3A). DTT treatment of the same

241 sample retarded the migration to the exact location as the PhoQ monomer, excluding the
242 likelihood of protein degradation. Nearly no PhoQ dimer band was detected under this
243 condition, further supporting that the orientation of the 188C side chain was more toward the
244 TM1 helix of the same protomer. In the presence of MgrB, the crosslinking pattern changed. The
245 intramolecular crosslinking band reduced, and the intensity of the PhoQ dimer band increased
246 (Fig. 3A, S6C). In this case, crosslinked PhoQ dimer could be formed in four ways: 43C-43'C, 43C-
247 188'C, 43'C-188C, and 188C-188'C. Our control samples showed that the crosslinking was
248 reduced for 43C-43'C and 188C-188'C when MgrB was present. Therefore, the increase in PhoQ
249 dimer formation was likely due to the inter-monomeric crosslinking between positions 43 and
250 188, suggesting that the binding of MgrB changes the crosslinking pattern from intra- to inter-
251 monomeric linkage and likely the relative orientation between PhoQ residue 188 to residue 43
252 (Fig. 3B). We also observed a similar trend of change in crosslinking for the residue 43 and 187
253 pair but with reduced intramolecular crosslinking efficiency (Fig. S6C). Taken together, we
254 hypothesize that MgrB may promote a rotational or translational movement of one TM2
255 periplasmic terminus towards the TM1 from the other promoter. Because the stoichiometry of
256 PhoQ and MgrB remains unknown, whether the conformational change detected here occurs in
257 both PhoQ protomers awaits further investigations.
258
259 **MgrB repression of PhoQ is divergent from high magnesium repression**
260 Besides the small protein MgrB, high magnesium also represses PhoQ kinase activity [14]. The
261 structural change of PhoQ under magnesium repression was studied in detail by monitoring the
262 arrangement of α helices along the PhoQ dimer interface via disulfide crosslinking [36]. It was
263 proposed that under high magnesium conditions, the N-terminal α helix across the TM and the
264 periplasmic domains undergoes a scissoring-type of motion with the pivot point near the
265 periplasm/membrane interface [36].
266
267 Using a similar approach, we monitored the arrangement of α helices along the PhoQ dimer
268 interface in the presence and absence of MgrB. Our data showed that most TM1 residues had
269 reduced crosslinking between PhoQ protomers upon MgrB binding (Fig. 3C blue residues, Fig.
270 S7). This reduction was more prominent for residues close to the cytoplasm, suggesting that
271 MgrB binding pushes TM1-TM1' apart and the propagation of PhoQ conformational change
272 from the periplasm to the cytoplasm. In contrast, the presence of MgrB did not show a similar
273 crosslinking effect on residues along the periplasmic helical interface (Fig. 3C purple residues,
274 Fig. S7). Most residues in this region showed little change in the crosslinking pattern. Some
275 showed a significantly decreased (i.e., residues 46 and 60) or a slightly increased dimer fraction
276 (i.e., residues 62). The overall PhoQ dimer rearrangement upon MgrB binding differed from the
277 scissoring motion proposed for high magnesium repression, suggesting that MgrB and high
278 magnesium act differently on PhoQ. We then did functional analyses of PhoQ under high
279 magnesium, with MgrB, or with both repressive factors. The results showed that PhoQ was
280 further repressed significantly when both high magnesium and MgrB were present (Fig. 3D),
281 supporting the hypothesis that magnesium and MgrB may have divergent mechanisms of
282 repression.
283
284 **Molecular dynamics simulations of PhoQ/MgrB complex models**
285 When comparing the predicted PhoQ dimer with its complex with MgrB, there was only minor
286 conformational change, which is in stark contrast to our experimental results. The Alphafold2
287 prediction might have only captured a transient arrangement of the complex but not the final
288 state. To investigate the effect of MgrB on the conformation of PhoQ in silico, we carried out a

289 set of four molecular dynamic simulations. The initial atomic models were obtained using the
290 best-ranked model predicted by the multimeric version of Alphafold2. In total, we modeled four
291 different complexes: PhoQ dimer (i) alone, and interacting with (ii) the wild-type MgrB, (iii) MgrB
292 W20Y, and (iv) MgrB W20A. Each complex was inserted into a bacterial mimetic membrane
293 bilayer, and simulations were carried out up to 1 µs under near-physiological conditions. To
294 evaluate the impact of the starting conformation on the stability of the PhoQ/MgrB complex, we
295 carried out two additional 500 ns simulations seeded from the second and third predictions. All
296 protein complexes remained stable throughout the entire simulations, with minor fluctuation in
297 the secondary structure. We did not observe any significant differences between the three
298 PhoQ/MrgB simulations. The MgrB C-terminal short helix (A40-W47) was buried close to the
299 membrane surface. The C-terminal carboxylate group interacted with the head group of PE
300 lipids in the simulations. The orientation of this C-terminal helix was primarily restrained by the
301 disulfide linkage (C28-C39) and remained stable in the simulations. A principal component
302 analysis of the transmembrane domain clearly showed that the functional MgrB variants (WT
303 and W20Y) induced a similar conformational change (Fig. 4A), corresponding to an increase in
304 the distance between PhoQ TM1 helices, coupled with a decrease in distance between TM2
305 helices. This change is more evident in TM residues near the membrane/cytoplasm interface
306 (Fig. 4B, S8). The MgrB W20A had only a marginal impact on the conformation of the
307 transmembrane domain.
308
309 In all the simulations with MgrB variants, we also observed the translocation of one of the PhoQ
310 catalytic-ATP binding (CA) domains (Fig. 4C). This is most prominent in the 1 µs simulations with
311 the wild-type MgrB, where one CA domain moved fully away from the helix harboring the
312 phosphorylatable histidine and located itself close to the inner membrane. For PhoQ alone, we
313 did not observe any significant movement of the CA domains throughout the entire simulation.
314 The functionally impaired MgrB W20A also induced PhoQ CA domain movement, though to a
315 lesser extent compared to the wild type (Fig. 4C). In this simulation, the CA domain remained
316 close to its initial position but rotated by about 90°. Our previous work showed that the W20A
317 mutant had low activity due to reduced affinity to PhoQ [30]. However, since the simulation was
318 seeded with a complex where MgrB W20A was already interacting with PhoQ, this likely
319 represents the scenario where overexpression of MgrB W20A compensates for its weak binding
320 to PhoQ and partially recovers its inhibitory function.
321
322 Overall, the simulation results confirm our experimental observations, showing the PhoQ
323 structural changes at the MgrB binding site. Furthermore, MgrB induces movements of the
324 distantly located CA domain, suggesting that the local conformational change due to MgrB
325 binding results in the repression of PhoQ kinase activity.
326
327 **MgrB mediates PhoQ sensing cationic antimicrobial peptides**
328 Our crosslinking data (Fig. 2B) suggested that MgrB directly interacts with PhoQ E184, a residue
329 involved in CAMP sensing [9]. We, therefore, hypothesized that MgrB might affect PhoQ
330 activation by CAMPs. To investigate this as well as the impact of MgrB on PhoQ sensing other
331 stimuli, we tested PhoQ activation by cationic antimicrobial peptides, low pH, and high
332 osmolarity in the presence and absence of MgrB (Fig. 5). Under a repressive magnesium
333 condition (LB medium supplemented with 10 mM Mg^{2+}), only slight or no PhoQ activation was
334 detected by antimicrobial peptide C18G regardless of MgrB, consistent with previous work
335 where high magnesium repressed the activation of PhoQ by CAMPs in *Salmonella* [9, 10].
336 Conversely, with the same magnesium condition (10 mM), a relatively large activation of PhoQ

337 was detected by low pH or osmolarity upshift in the presence of MgrB. The activation did not
338 appear to have a qualitative change when MgrB was absent, except that the overall PhoQ
339 activity increased due to the lack of MgrB repression (Fig. 5A).
340
341 We next followed PhoQ activities in the presence of antimicrobial peptide LL37 and C18G under
342 a physiologically relevant magnesium concentration (1 mM Mg^{2+} in LB) that does not repress
343 CAMPs from inducing PhoQ activity [9]. Up to a nearly 5-fold increase of PhoQ activity by
344 antimicrobial peptides was detected when the wild-type MgrB was present (Fig. 5B). However,
345 in the absence of MgrB, there was no significant further increase of PhoQ activity in the
346 presence of C18G. In the case of LL37, only a marginal increase (1.14-fold) of PhoQ activity was
347 observed, consistent with a previous report [15], suggesting that LL37 may be slightly different
348 from C18G in terms of PhoQ activation. To test if PhoQ was already maximally activated in the
349 *ΔmgrB* strain with 1 mM magnesium, we treated the cells with additional stimuli. PhoQ activity
350 was significantly further increased by lowered pH or elevated osmolarity (Fig. S9A), indicating
351 that PhoQ activity did not reach saturation with 1 mM magnesium alone. To be precise on the
352 total magnesium concentration in the growth medium, we tested our strains in the defined
353 minimal A medium [37] supplemented with 1 mM magnesium. Consistent with what we
354 observed in LB, PhoQ activity was higher in the absence of MgrB but could not be further
355 increased by C18G. Therefore, we hypothesize that MgrB may mediate PhoQ to sense
356 antimicrobial peptides under a physiologically relevant magnesium concentration.
357
358 The lack of PhoQ activation by antimicrobial peptides in the absence of MgrB might also be due
359 to the protective effect of the overall elevated activity of the PhoQ/PhoP two-component
360 system, which could increase the outer membrane modification and reduce the entry of
361 antimicrobial peptides to the periplasm. To obtain more direct evidence, we monitored PhoQ
362 and MgrB interactions *in vivo* using the acceptor photobleaching Förster resonance energy
363 transfer (FRET) approach. Functional PhoQ-mNeonGreen and mCherry-MgrB fusion proteins
364 (Fig. S9C and D) were expressed in *E. coli*. Cells were collected in the mid-log phase, treated with
365 C18G, and then used for FRET measurements (Fig. 5C). The control cells without C18G
366 treatment, showed energy transfer from mNeonGreen to mCherry with about 10% efficiency,
367 comparable to our previous report [12], indicating the formation of the PhoQ/MgrB complex *in*
368 *vivo*. With the C18G treatment, the FRET efficiency reduced to about 2%, slightly higher than the
369 negative controls, suggesting that C18G induces the dissociation of the PhoQ/MgrB complex.
370
371 To confirm the *in vivo* FRET results, we performed disulfide crosslinking experiments with or
372 without C18G using the PhoQ I38C MgrB F24C variant pair. We chose this pair because: i) they
373 formed a good amount of PhoQ/MgrB crosslinked complex readily detectable by Western blot
374 (Fig. 1F); ii) PhoQ I38C showed wild-type-like activity (Fig. 1F); iii) MgrB F24C repressed PhoQ
375 I38C to a relatively low level (Fig. 1F); iv) the variant pair responded to C18G showing
376 significantly increased PhoQ activity (Fig. 5D). Compared to the crosslinking in the absence of
377 C18G, we observed a lighter band corresponding to the PhoQ/MgrB complex (Fig. 5E). Assuming
378 that C18G does not adversely affect Cu: phenanthroline catalysis, the reduction in the
379 crosslinked complex suggests that C18G induces MgrB to move away from PhoQ, consistent
380 with our FRET results.
381
382 Taken together, we propose that MgrB is involved in PhoQ sensing CAMPs. Under
383 physiologically relevant magnesium conditions, PhoQ is active but partially repressed due to the
384 bound MgrB. This state allows PhoQ to detect and respond sensitively to CAMPs at a sub-

inhibitory concentration. CAMPs bind to PhoQ and induce the release of the bound MgrB, further activating PhoQ/PhoP-regulated genes and potentially increasing bacterial resistance to CAMPs (Fig. 6).

Discussion

In this study, we report that MgrB directly interacts with the TM helices and the periplasmic/TM linker region of PhoQ, changing its conformation in a way that divergent from high magnesium repression. It reduces the overall activity of PhoQ yet still allows its activation by low magnesium, low pH, and increased osmolarity. We further reveal that PhoQ activation by CAMPs is MgrB-dependent under physiologically relevant magnesium conditions. CAMPs induce MgrB dissociating from PhoQ and thus increase PhoQ activity via derepression. A higher PhoQ activity leads to an increased outer membrane modification and improved resistance to CAMPs. Since the septum is the initial attacking site of certain CAMPs (i.e., LL37) on the membrane [38], the possible division block caused by strong PhoQ activation may also protect bacteria against the host's innate immune response. CAMPs were suggested to bind to an acidic surface in the PhoQ periplasmic domain, though the exact binding site has not been well defined [9]. The acidic cluster (^{148}EDDDDAE), a major component of the acidic surface, is relatively distant from the MgrB binding site. However, it remains unclear whether the acidic residue E184 in the linker region is directly involved in CAMP binding. It is plausible that the binding of CAMPs induces PhoQ conformational change, which leads to the dissociation of MgrB from PhoQ.

We observed that a high level of magnesium (10 mM) repressed PhoQ activation by CAMPs in the presence or absence of MgrB in *E. coli*, consistent with a previous report on PhoQ in *Salmonella*, though MgrB had not yet been discovered at that time [9]. The same report proposed that CAMPs activate PhoQ by replacing magnesium ions from the acidic cluster in PhoQ, which is different from our MgrB-mediated CAMP sensing mechanism. Both hypotheses, however, do not conflict with each other but rather describe two aspects of PhoQ sensing CAMPs under different magnesium conditions. It is also possible that magnesium may affect MgrB binding to PhoQ, thus connecting these two mechanisms of CAMP sensing by PhoQ. Interestingly, the magnesium replacement mechanism can not explain PhoQ activation by antimicrobial peptides in some cases. For example, a recent study revealed that antimicrobial peptides with a ß-sheet structure or a neutral charge could also activate PhoQ [39]. These newly found PhoQ activators do not possess the properties to interact with the PhoQ acidic cluster. Furthermore, there are PhoQ homologs that do not contain an acidic cluster in their sequences. Our MgrB-dependent antimicrobial peptide sensing mechanism may provide a suitable explanation for both cases.

By monitoring PhoQ conformational change and activities, we show that MgrB repression diverges from high magnesium repression. This is consistent with the different binding sites of magnesium and MgrB on PhoQ. Magnesium was suggested to bind to several locations, including the acidic cluster near the inner membrane (148-152) and residues G93, W97, H120, and T156 [14, 23, 40]. Mutations of these residues were shown to abolish magnesium protection from iron-mediated protein cleavage [40]. The majority of these residues are located in the peripheral of the periplasmic domain, distinct from the MgrB binding site.

Our crosslinking results revealed extensive interactions between MgrB and the PhoQ linker region, implying its importance in functional regulations. Highly conserved and functionally

433 important residues are found in or near this region, such as K186, T48, R50, E184, and L185,
434 mutations of which lead to alterations in PhoQ activity as well as signaling capability [20, 23, 24].
435 Curiously, the wild-type MgrB maintained its inhibition on PhoQ linker variants, suggesting that
436 the flexible MgrB loop may have various interaction modes with the PhoQ linker region.
437 Interestingly, the PhoQ activating protein, SafA, appears to act near this linker region in terms of
438 the putative SafA binding site, and the activation required inter-monomeric salt bridge (R50'-
439 D179) [41, 42]. Whether MgrB repression competes with SafA activation of PhoQ and how these
440 regulations are coordinated await further studies.
441
442 Sensor kinases in bacterial two-component systems are evolutionarily related and have
443 structural resemblance. We found that the predicted structures of EnvZ, QseC, and CreC sensor
444 kinases closely resemble the PhoQ structure. EnvZ was also shown to form a complex with MgrB
445 experimentally [30]. With the mechanism of MgrB revealed here, it is foreseeable that novel
446 small protein regulators can be designed for PhoQ, EnvZ, and possibly many other sensor
447 kinases. This will contribute to the repertoire of new antimicrobial agents targeting sensor
448 kinases that regulate bacterial virulence [43] and to the treatment of infections caused by drug-
449 resistant pathogens.
450
451 **Materials and methods**
452
453 **Bacterial strains, plasmids, and growth conditions**
454 The complete lists of strains, plasmids, and primers used in this study are summarized in Table
455 S1, S2, and S3, respectively. The *E. coli* MG1655 *ΔmgrB* and *ΔphoQΔmgrB* strains were from the
456 previous study [30]. All strains were grown in the lysogeny broth (LB) medium or minimal A
457 medium [37] containing 0.2% glycerol, 0.1% casamino acids supplemented with magnesium as
458 indicated. Cells were grown at 37 ^{o}C with shaking unless otherwise indicated. Genes in pTrc99a
459 vector were induced with isopropyl β-D-1-thiogalactopyranoside (IPTG) at a final concentration
460 of 10 µM. Genes in pBAD vector were induced with 0.008% arabinose. Genes in pEVOL-pBpF
461 vector were induced with 0.02% arabinose. Genes in pETduet-1 vector were induced with IPTG
462 at a final concentration of 0.5 mM. When appropriate, the antibiotics ampicillin, kanamycin, and
463 chloramphenicol were used at concentrations of 100 µg/ml, 50 µg/ml, and 34 µg/ml,
464 respectively. A detailed description of cloning and plasmid construction can be found in the SI
465 Materials and Methods.
466
467 **Disulfide crosslinking *in vivo***
468 The *in vivo* disulfide-crosslinking experiments were performed as previously described with
469 modifications [44]. Briefly, cells carrying pBAD33 *phoQ* variant and pTrc99A *mgrB* variant were
470 grown at 37 °C in LB medium supplemented with 10 mM $MgSO_4$ overnight, then diluted 1:100 to
471 fresh LB medium supplemented with 1 mM $MgSO_4$. The expression of plasmid-encoded proteins
472 was induced with arabinose and IPTG. When the OD_{600} value reached 0.6, cells were harvested,
473 washed, and resuspended in the crosslinking buffer (137 mM NaCl, 2.7 mM KCl, 10 mM
474 Na_2HPO_4, 1.8 mM KH_2PO_4, 1 mM $MgSO_4$, and 0.1 mM Cu-phenanthroline), followed by 10
475 minutes incubation at 25 °C. The reaction was stopped by pelleting the cells and then
476 resuspending in the 1x stop-solution (8 mM sodium phosphate buffer, pH 7.8, 12.5 mM EDTA,
477 and 12.5 mM N-ethylmaleimide) and incubation at 25 °C for 10 minutes. Cells were collected,
478 resuspended in the lysis buffer (50 mM Tris-HCl, pH 8.0, 100 mM NaCl, and protease inhibitors),
479 mixed with lysing matrix B beads (MP Biomedicals), and broken with a homogenizer following
480 the manufacturer's instructions. The mixture was spun down at 2,300 x g for 10 minutes at 4 °C

481 to pellet the beads and cell debris. The supernatant was centrifuged at 21,000 x g for one hour
482 at 4 °C to pellet the membrane fraction, which was then dissolved in the SDS sample buffer at 4
483 °C overnight. The membrane proteins were separated on an SDS tris-tricine or tris-glycine
484 polyacrylamide gel via electrophoresis and analyzed with Western blot.
485
486 **Western blot analysis**
487 Proteins were transferred from a polyacrylamide gel to a polyvinylidene fluoride membrane or
488 nitrocellulose membrane. PhoQ-His and Flag-MgrB were detected with the anti-His and anti-Flag
489 primary antibody (Sigma), respectively. The IRDye 800CW-conjugated secondary antibody (LI-
490 COR) was used, and the protein bands were visualized with the Odyssey CLx imaging system (LI-
491 COR) and quantified with ImageJ. The crosslinking efficiency was calculated by dividing the
492 amount of PhoQ/MgrB complex with the total amount of PhoQ/MgrB complex and MgrB
493 monomer.
494
495 **Functional assay with the *gfp* reporter gene**
496 The GFP reporter assay was performed as a previous study [12]. Briefly, the reporter plasmid
497 pUA66 P_{mgtLA}-*gfp* was transformed to strains indicated. The resulting transformants were grown
498 overnight at 37 °C in LB medium with 10 mM $MgSO_4$, then diluted 1:100 to fresh LB medium
499 with magnesium and/or stimuli as indicated. The cultures were grown at 37 °C with vigorous
500 shaking till the early log phase (OD=0.4-0.5). The fluorescence of cells was monitored with a BD
501 LSRFortessa SORP flow cytometer (BD Biosciences) equipped with a 100-mW 488-nm laser and a
502 510/20 bandpass filter. BD FACSDiva software version 8.0 (BD Biosciences) was used to analyze
503 the acquired data.
504
505 **Unnatural amino acid incorporation in MgrB and site-specific UV crosslinking *in vivo***
506 The site-specific photo-crosslinking experiments were performed as previous studies with
507 modifications [35, 45]. *E. coli* BL21 DE3 cells carrying pETduet-1 *phoQ-his*$_6$ *flag-mgrB* and pEVOL-
508 pBpF vectors were grown in LB medium at 37 °C overnight, then diluted 1:100 to fresh LB
509 medium containing 0.5 mM *p*Bpa. When the OD_{600} value reached around 0.6, cells were induced
510 with arabinose (0.02%) and IPTG (0.5 mM) for 4h at 30 °C, followed by harvesting, washing two
511 times, and resuspension in 1 ml cold PBS buffer. The bacterial suspension was spread out onto a
512 35 mm round dish on ice and irradiated for 5 minutes with 365 nm UV light using an LED UV
513 hand lamp (Honle UV technology). Cells were then harvested at 4 °C, and the formation of
514 crosslinked PhoQ/MgrB complex was then detected by the separation of total protein with
515 polyacrylamide gel electrophoresis and Western blot with anti-Flag antibody. The crosslinked
516 complex was purified by affinity chromatography, separated in an SDS polyacrylamide gel, and
517 verified by mass spectrometry (see SI Materials and Methods for details).
518
519 **Molecular Modeling and Molecular Dynamics simulations**
520 The PhoQ/MgrB complex was modeled using Alphafold2 multimer on Colab [PMID: 35637307].
521 We considered six different complexes: i. PhoQ, ii. PhoQ / MgrB (predictions ranked 1 to 3), iii.
522 PhoQ / MgrB W20Y variant, and iv. PhoQ / MgrB W20A variant. Each complex was inserted into
523 a bacterial membrane mimetic composed of a mixture of phosphatidylethanolamine (POPE) and
524 phosphatidylglycerol (POPG) with a 3:1 ratio. The systems were solvated with a 17 Å water
525 padding and neutralized with NaCl at a concentration of 150 mM. Each system was assembled
526 using the CHARMM-GUI webserver [46].
527

528 The simulation was performed with the CHARMM36m force field, including CMAP corrections
529 for the protein [47]. The water molecules were described with the TIP3P water parameterization
530 [48]. The simulations were carried out with OPENMM molecular engine [49] following the
531 minimization and equilibration protocols provided by CHARMM-GUI. The cutoff for non-bonded
532 interactions was set to 12 Å with a switching distance at 10 Å. The periodic electrostatic
533 interactions were computed using particle-mesh Ewald (PME) summation with a grid spacing
534 smaller than 1 Å. Constant temperature of 310 K was imposed by Langevin dynamics with a
535 damping coefficient of 1.0 ps. Constant pressure of 1 atm was maintained with Monte Carlo
536 barostat [50]. The hydrogen mass repartitioning scheme was used to achieve a 4 fs time-step
537 [51]. Each simulation was carried out up to 1 µs and up to 500 ns for the second and third
538 ranked predictions of PhoQ / MgrB.
539
540 **Acceptor photobleaching FRET analysis**
541 FRET measurements were performed as described before [30]. The expression of PhoQ-
542 mNeonGreen and mCherry-MgrB was induced in *E. coli* lptD4213 strain with 0.008% arabinose
543 and 10 µM IPTG, respectively. The cultures were grown to the mid-log phase (OD=0.6) in LB
544 media. Cells were harvested and washed twice with pre-chilled tethering buffer (20 mM
545 potassium phosphate pH 7.0, 1 µM methionine, and 10 mM lactic acid). The surface of a glass-
546 bottom 96-well plate (Greiner) was treated with 0.1% poly-L-lysine for 15 minutes at room
547 temperature, followed by removing poly-L-Lysine and air-dry for 5 minutes. The wells were
548 washed twice using a pre-chilled tethering buffer. Subsequently, cells were incubated in the
549 wells at room temperature for 25 minutes to allow attachment. Unattached cells were removed
550 by washing with tethering buffer twice, and attached cells were overlaid with tethering buffer
551 with or without 10 µg/ml C18G and incubated at room temperature for one hour. Acceptor
552 photobleaching FRET was performed using the same microscope settings previously [30]. The
553 details of the data acquisition and analysis can be found in the SI Materials and Methods.
554
555
556 **Acknowledgments**
557 We thank L. Cassidy and A. Throley (the Christian-Albrecht University of Kiel) for performing
558 mass spectrometry analyses, writing and editing the manuscript; H. Koch (the Albert Ludwig
559 University of Freiburg) for pEVOL-pBpF vector and the site-directed photo-crosslinking protocol;
560 M. Stopp for the disulfide crosslinking protocol; S. G. Sierra for technical assistance; members of
561 the Yuan and the Sourjik laboratories for helpful discussions.
562
563 We thank G. Storz (National Institutes of Health), V. Sourjik (Max Planck Institute for Terrestrial
564 Microbiology), R. Lill (Philipps University of Marburg), and S. Yadavalli (Rutgers University) for
565 their suggestions to improve the manuscript.
566
567 This work is supported by the German Research Foundation (DFG) priority program 2002 YU
568 247/3-1 and the Max Planck Society (to J.Y.), the Swiss National Science Foundation (SNSF) grant
569 PCEFP3_194606 (to T.L. and S.L.).
570
571 J.Y. and T.L. designed the experiments; S.J., L.C.S., C.K., S.L., and J.Y. performed the experiments;
572 S.J., G.M., L.C.S., C.K., S.L., T.L., V.S., and J.Y. analyzed data; J.Y., T.L., and S.J. wrote the
573 manuscript.
574
575 **References**

576
577 1. Duval, M. and P. Cossart, *Small bacterial and phagic proteins: an updated view*
578 *on a rapidly moving field.* Curr Opin Microbiol, 2017. **39**: p. 81-88.
579 2. Ramamurthi, K.S. and G. Storz, *The small protein floodgates are opening; now*
580 *the functional analysis begins.* BMC Biol, 2014. **12**: p. 96.
581 3. Su, M., et al., *Small proteins: untapped area of potential biological importance.*
582 Front Genet, 2013. **4**: p. 286.
583 4. Weidenbach, K., et al., *Small Proteins in Archaea, a Mainly Unexplored World.* J
584 Bacteriol, 2022. **204**(1): p. e0031321.
585 5. Sberro, H., et al., *Large-Scale Analyses of Human Microbiomes Reveal Thousands*
586 *of Small, Novel Genes.* Cell, 2019. **178**(5): p. 1245-1259 e14.
587 6. Hemm, M.R., J. Weaver, and G. Storz, *Escherichia coli Small Proteome.* EcoSal
588 Plus, 2020. **9**(1).
589 7. Yadavalli, S.S. and J. Yuan, *Bacterial Small Membrane Proteins: the Swiss Army*
590 *Knife of Regulators at the Lipid Bilayer.* J Bacteriol, 2022. **204**(1): p. e0034421.
591 8. Groisman, E.A., A. Duprey, and J. Choi, *How the PhoP/PhoQ System Controls*
592 *Virulence and Mg(2+) Homeostasis: Lessons in Signal Transduction, Pathogenesis,*
593 *Physiology, and Evolution.* Microbiol Mol Biol Rev, 2021. **85**(3): p. e0017620.
594 9. Bader, M.W., et al., *Recognition of antimicrobial peptides by a bacterial sensor*
595 *kinase.* Cell, 2005. **122**(3): p. 461-72.
596 10. Prost, L.R., et al., *Activation of the bacterial sensor kinase PhoQ by acidic pH.* Mol
597 Cell, 2007. **26**(2): p. 165-74.
598 11. Choi, J. and E.A. Groisman, *Acidic pH sensing in the bacterial cytoplasm is*
599 *required for Salmonella virulence.* Mol Microbiol, 2016. **101**(6): p. 1024-38.
600 12. Yuan, J., et al., *Osmosensing by the bacterial PhoQ/PhoP two-component system.*
601 Proc Natl Acad Sci U S A, 2017. **114**(50): p. E10792-E10798.
602 13. Carabajal, M.A., et al., *PhoQ is an unsaturated fatty acid receptor that fine-tunes*
603 *Salmonella pathogenic traits.* Sci Signal, 2020. **13**(628).
604 14. Garcia Vescovi, E., F.C. Soncini, and E.A. Groisman, *Mg^{2+} as an extracellular*
605 *signal: environmental regulation of Salmonella virulence.* Cell, 1996. **84**(1): p.
606 165-74.
607 15. Lippa, A.M. and M. Goulian, *Feedback inhibition in the PhoQ/PhoP signaling*
608 *system by a membrane peptide.* PLoS Genet, 2009. **5**(12): p. e1000788.
609 16. Eguchi, Y., et al., *B1500, a small membrane protein, connects the two-component*
610 *systems EvgS/EvgA and PhoQ/PhoP in Escherichia coli.* Proceedings of the
611 National Academy of Sciences of the United States of America, 2007. **104**(47): p.
612 18712-18717.
613 17. Yadavalli, S.S., et al., *Antimicrobial peptides trigger a division block in Escherichia*
614 *coli through stimulation of a signalling system.* Nat Commun, 2016. **7**: p. 12340.
615 18. Eguchi, Y., et al., *Regulation of acid resistance by connectors of two-component*
616 *signal transduction systems in Escherichia coli.* J Bacteriol, 2011. **193**(5): p. 1222-
617 8.
618 19. Salvail, H., J. Choi, and E.A. Groisman, *Differential synthesis of novel small protein*
619 *times Salmonella virulence program.* PLoS Genet, 2022. **18**(3): p. e1010074.

620 20. Sanowar, S., A. Martel, and H.L. Moual, *Mutational analysis of the residue at*
621 *position 48 in the Salmonella enterica Serovar Typhimurium PhoQ sensor kinase.*
622 J Bacteriol, 2003. **185**(6): p. 1935-41.
623 21. Regelmann, A.G., et al., *Mutational analysis of the Escherichia coli PhoQ sensor*
624 *kinase: differences with the Salmonella enterica serovar Typhimurium PhoQ*
625 *protein and in the mechanism of Mg2+ and Ca2+ sensing.* J Bacteriol, 2002.
626 **184**(19): p. 5468-78.
627 22. Minagawa, S., et al., *Isolation and molecular characterization of the locked-on*
628 *mutant of Mg2+ sensor PhoQ in Escherichia coli.* Biosci Biotechnol Biochem,
629 2005. **69**(7): p. 1281-7.
630 23. Cho, U.S., et al., *Metal bridges between the PhoQ sensor domain and the*
631 *membrane regulate transmembrane signaling.* J Mol Biol, 2006. **356**(5): p. 1193-
632 206.
633 24. Cheung, J., et al., *Crystal structure of a functional dimer of the PhoQ sensor*
634 *domain.* J Biol Chem, 2008. **283**(20): p. 13762-70.
635 25. Waldburger, C.D. and R.T. Sauer, *Signal detection by the PhoQ sensor-*
636 *transmitter. Characterization of the sensor domain and a response-impaired*
637 *mutant that identifies ligand-binding determinants.* J Biol Chem, 1996. **271**(43):
638 p. 26630-6.
639 26. Venturini, E.S., S. L.; Maaß, S.; Gelhausen, R.; Eggenhofer, F.; Li, L.; Cain, A. K.;
640 Parkhill, J.; Becher, D.; Backofen, R.; Barquist, L.; Sharma, C. M.; Westermann, A.
641 J.; Vogel, J., *A global data-driven census of Salmonella small proteins and their*
642 *potential functions in bacterial virulence.* microLife, 2020. **1**(1).
643 27. Shein, A.M.S., et al., *High prevalence of mgrB-mediated colistin resistance among*
644 *carbapenem-resistant Klebsiella pneumoniae is associated with biofilm*
645 *formation, and can be overcome by colistin-EDTA combination therapy.* Sci Rep,
646 2022. **12**(1): p. 12939.
647 28. Salazar, M.E., A.I. Podgornaia, and M.T. Laub, *The small membrane protein MgrB*
648 *regulates PhoQ bifunctionality to control PhoP target gene expression dynamics.*
649 Mol Microbiol, 2016. **102**(3): p. 430-445.
650 29. Lippa, A.M. and M. Goulian, *Perturbation of the oxidizing environment of the*
651 *periplasm stimulates the PhoQ/PhoP system in Escherichia coli.* J Bacteriol, 2012.
652 **194**(6): p. 1457-63.
653 30. Yadavalli, S.S., et al., *Functional determinants of a small protein controlling a*
654 *broadly conserved bacterial sensor kinase.* J Bacteriol, 2020.
655 31. Mirdita, M., et al., *ColabFold: making protein folding accessible to all.* Nat
656 Methods, 2022. **19**(6): p. 679-682.
657 32. Evans, R., et al., *Protein complex prediction with AlphaFold-Multimer.* bioRxiv,
658 2022: p. 2021.10.04.463034.
659 33. Akdel, M., et al., *A structural biology community assessment of AlphaFold2*
660 *applications.* Nat Struct Mol Biol, 2022.
661 34. Ferris, H.U., et al., *Mechanism of regulation of receptor histidine kinases.*
662 Structure, 2012. **20**(1): p. 56-66.

663 35. Ryu, Y. and P.G. Schultz, *Efficient incorporation of unnatural amino acids into*
664 *proteins in Escherichia coli.* Nat Methods, 2006. **3**(4): p. 263-5.
665 36. Molnar, K.S., et al., *Cys-scanning disulfide crosslinking and bayesian modeling*
666 *probe the transmembrane signaling mechanism of the histidine kinase, PhoQ.*
667 Structure, 2014. **22**(9): p. 1239-1251.
668 37. Miller, J.H., *A Short Course in Bacterial Genetics - A Laboratory Manual and*
669 *Handbook for Escherichia coli and Related Bacteria.* 1992: Cold Spring Harbor
670 Laboratory Press.
671 38. Sochacki, K.A., et al., *Real-time attack on single Escherichia coli cells by the*
672 *human antimicrobial peptide LL-37.* Proc Natl Acad Sci U S A, 2011. **108**(16): p.
673 E77-81.
674 39. Brink, K.R., et al., *An E. coli display method for characterization of peptide-sensor*
675 *kinase interactions.* Nat Chem Biol, 2022.
676 40. Chamnongpol, S., M. Cromie, and E.A. Groisman, *Mg2+ sensing by the Mg2+*
677 *sensor PhoQ of Salmonella enterica.* J Mol Biol, 2003. **325**(4): p. 795-807.
678 41. Eguchi, Y., et al., *The connector SafA interacts with the multi-sensing domain of*
679 *PhoQ in Escherichia coli.* Mol Microbiol, 2012. **85**(2): p. 299-313.
680 42. Yoshitani, K., et al., *Identification of an internal cavity in the PhoQ sensor domain*
681 *for PhoQ activity and SafA-mediated control.* Biosci Biotechnol Biochem, 2019.
682 **83**(4): p. 684-694.
683 43. Cabezudo, I., et al., *Effect-Directed Synthesis of PhoP/PhoQ Inhibitors to Regulate*
684 *Salmonella Virulence.* J Agric Food Chem, 2022. **70**(22): p. 6755-6763.
685 44. Stopp, M., et al., *Transmembrane signaling and cytoplasmic signal conversion by*
686 *dimeric transmembrane helix 2 and a linker domain of the DcuS sensor kinase.* J
687 Biol Chem, 2021. **296**: p. 100148.
688 45. Kuhn, P., et al., *Ribosome binding induces repositioning of the signal recognition*
689 *particle receptor on the translocon.* J Cell Biol, 2015. **211**(1): p. 91-104.
690 46. Jo, S., et al., *CHARMM-GUI: a web-based graphical user interface for CHARMM.* J
691 Comput Chem, 2008. **29**(11): p. 1859-65.
692 47. Best, R.B., et al., *Optimization of the additive CHARMM all-atom protein force*
693 *field targeting improved sampling of the backbone phi, psi and side-chain chi(1)*
694 *and chi(2) dihedral angles.* J Chem Theory Comput, 2012. **8**(9): p. 3257-3273.
695 48. Jorgensen, W.L., Chandrasekhar, J., and Madura, J. D., *Comparison of simple*
696 *potential functions for simulating liquid water.* J Chem Phys, 1983. **79**(2).
697 49. Eastman, P., et al., *OpenMM 7: Rapid development of high performance*
698 *algorithms for molecular dynamics.* PLoS Comput Biol, 2017. **13**(7): p. e1005659.
699 50. Chow, K.a.F., D. M. , *Isothermal-isobaric molecular dynamics simulations with*
700 *Monte Carlo volume sampling.* Comp. Phys. Comm., 1995. **91**(1-3): p. 283-289.
701 51. Balusek, C., et al., *Accelerating Membrane Simulations with Hydrogen Mass*
702 *Repartitioning.* J Chem Theory Comput, 2019. **15**(8): p. 4673-4686.
703
704

705 **Figures and tables**

706

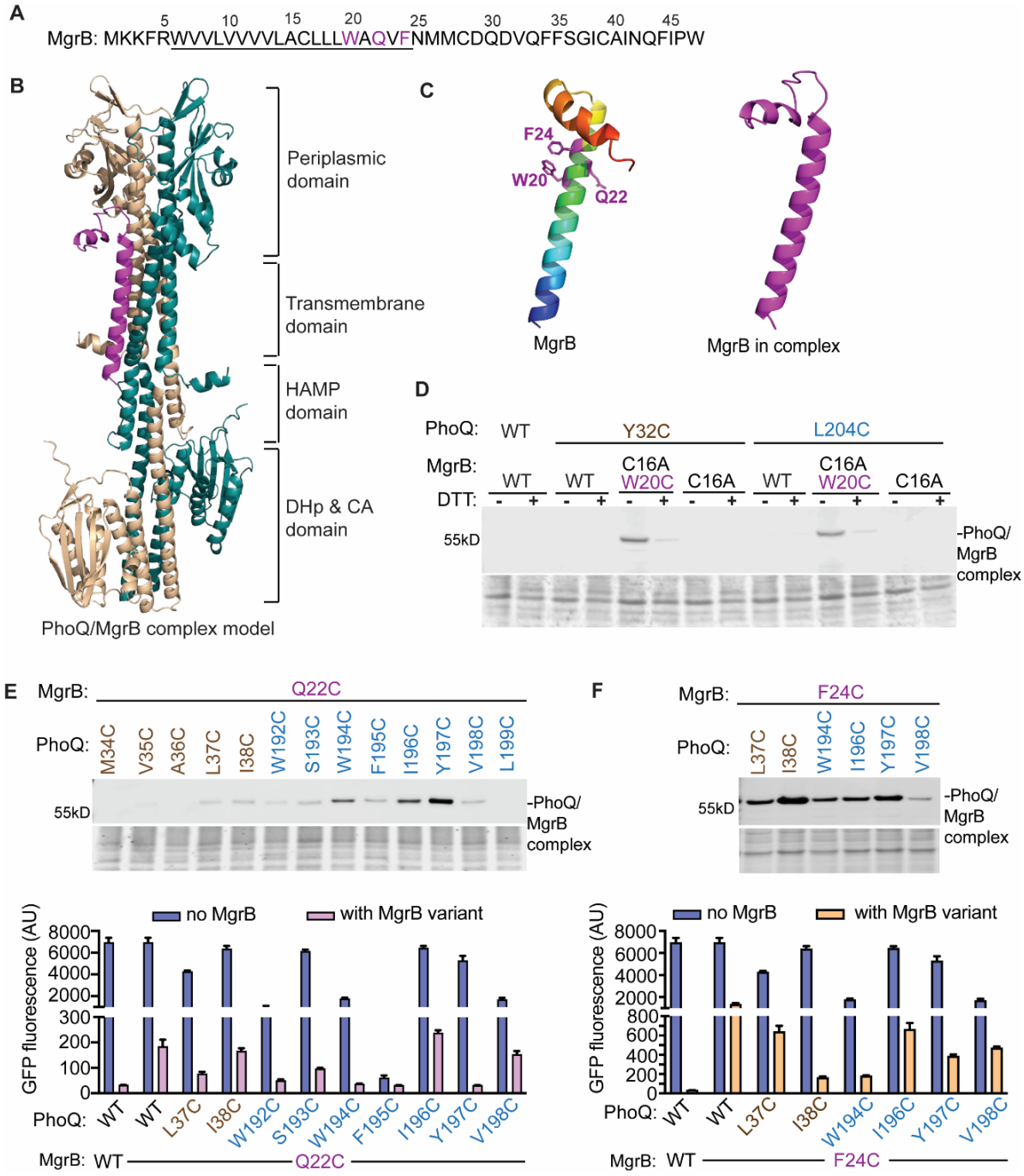

707
708

709 **Fig. 1. Identification of the interacting residues between MgrB and PhoQ in the**
710 **transmembrane helices.** (**A**) The sequence of MgrB from *E. coli*. Residues predicted to be in the
711 transmembrane helix are underlined. (**B**) The tertiary structure of the top ranked PhoQ/MgrB
712 complex predicted by Alphafold2. The two PhoQ protomers are colored in wheat and teal. MgrB
713 is colored in magenta. (**C**) The structural models of MgrB predicted by Alphafold2 are shown in
714 ribbon. The model of MgrB alone (left) is colored in rainbow spectrum with the N-terminus in
715 blue and the C-terminus in red. The positions involved in crosslinking (20, 22 and 24) are in

716 purple and shown with side chains in ball-and-stick. The predicted structure of MgrB in complex
717 (right) is colored in magenta. All structural figures were prepared using PyMOL unless otherwise
718 stated. (**D, E top, F top**) Western blot analysis of *E. coli* membrane extracts after disulfide
719 crosslinking. The indicated PhoQ and FLAG-tagged MgrB variants were expressed in *E. coli*,
720 followed by Cu-phenanthroline catalyzed disulfide crosslinking (details in Materials and
721 Methods). The total protein stain of the PVDF membranes serves as loading controls. Residues
722 from PhoQ TM1 and TM2 are colored in wheat and teal, respectively. Magenta indicates the
723 residues in the MgrB TM helix. Data are representative of at least three independent
724 experiments**. (D bottom, F bottom**) The functional assay of PhoQ Cys-variants with or without
725 MgrB. An GFP reporter plasmid carrying the *gfp* gene fused with a PhoP regulated promoter
726 P_{mgtLA} was introduced to the *E. coli* strain. The expression of *phoQ* and *mgrB* variants was
727 induced and cells were grown to the early log phase. The function of PhoQ variants was then
728 monitored by measuring the GFP fluorescence of the cell culture. Each data point is shown with
729 the calculated average and standard deviation from three independent biological replicates.
730

731

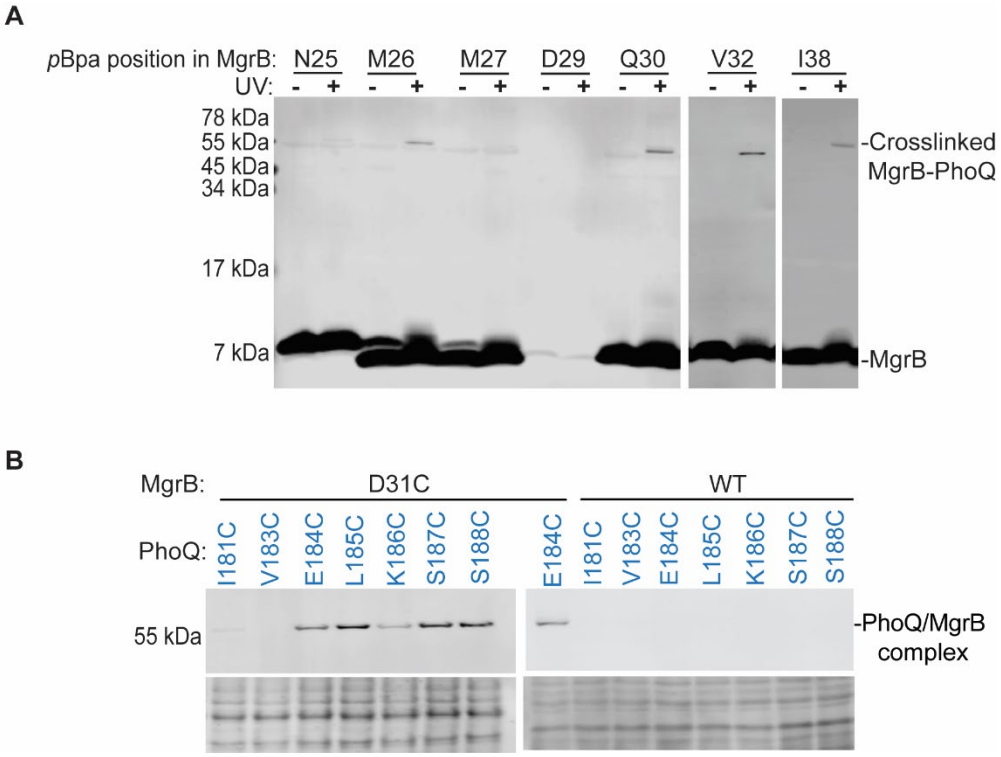

732
733
734
735 **Fig. 2. Site-specific photo crosslinking in the periplasmic domain.** (**A**) Western blot analysis of
736 the site-specific photo crosslinking between PhoQ and MgrB. The *E. coli ΔphoQΔmgrB* strain
737 harboring pETduet-1 *phoQ-his*$_6$ *flag-mgrB* and pEVOL-pBpF vectors were grown in LB containing
738 the unnatural amino acid, *p*Bpa, which was incorporated into the FLAG tagged MgrB at the
739 indicated positions via the amber stop codon and the cognate tRNA/aminoacyl-tRNA synthetase
740 pair. Cells were treated with UV light. The crosslinked MgrB-PhoQ complex was detected with
741 Western blot using antibodies directed to the FLAG epitopes. Samples without UV irradiation
742 served as controls. (**B**) Western blot analysis of disulfide crosslinking from MgrB residue 31 to
743 the PhoQ linker region connecting the periplasmic domain to the TM2 helix. The experimental
744 procedure is as in Fig. 1D and details can be found in Materials and Methods. Data are
745 representative of at least three independent experiments.
746

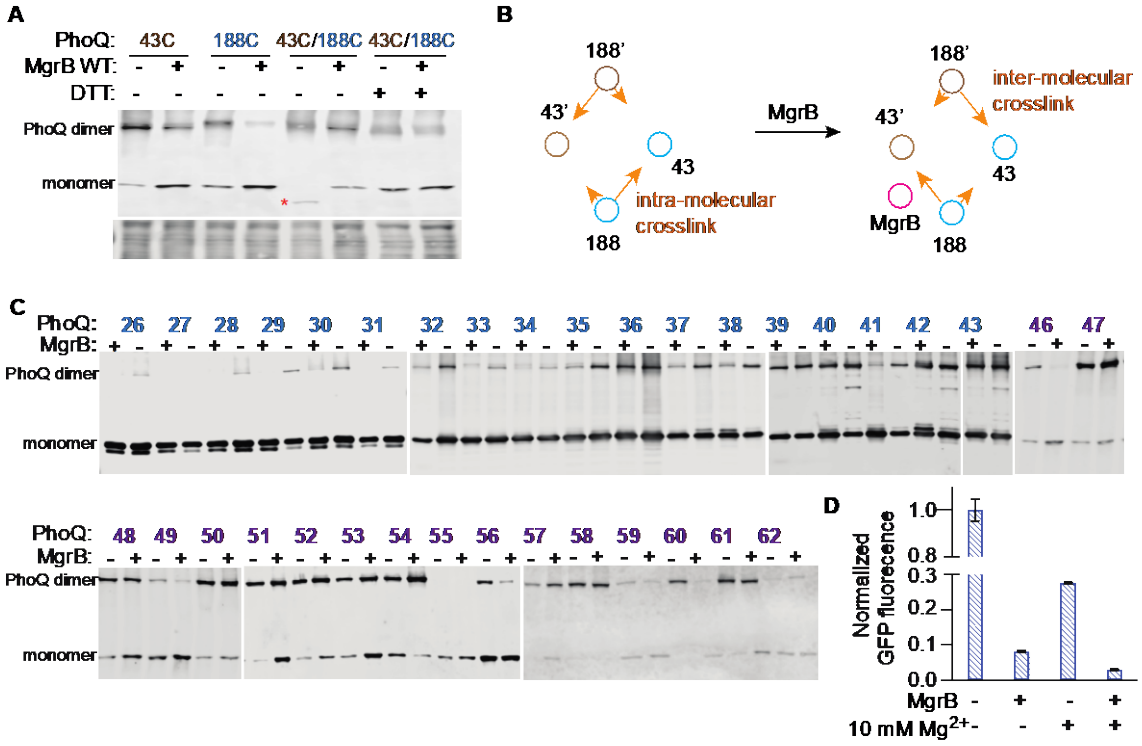

Fig. 3. The conformational change of the PhoQ sensor kinase upon MgrB binding. (**A**) Western blot analysis of disulfide crosslinking within the PhoQ molecule in the presence or absence of MgrB. The His_6-tagged PhoQ cysteine variants were expressed with or without the wild type MgrB in *E. coli*. The disulfide crosslinking reaction was initiated with Cu-phenanthroline. The resulting crosslinked PhoQ species was then detected using Western blot with an anti-His antibody. The red asterisk indicates PhoQ molecules with an intramolecular disulfide crosslink. The total protein stain serves as a loading control. Data are representative of three independent experiments. (**B**) A diagram of MgrB affecting the disulfide crosslinking between the cysteine residues at position 43 and 188. Brown and cyan circles represent the TM helices in each PhoQ monomer. The magenta circle represents MgrB. Orange arrows indicate the crosslinking tendency of Cys188 to Cys43 in the same or different PhoQ monomer. (**C**) MgrB induced PhoQ conformational change along the PhoQ dimer interface. The His_6-tagged PhoQ cysteine variants were expressed with or without the wild type MgrB in *E. coli*. The experimental procedure is as described in A and details can be found in Materials and Methods. The position of cysteine is indicated as residue numbers in the PhoQ N-terminal helix. Numbers colored in blue and purple are residues in TM and periplasmic domains, respectively. Data are representative of three independent experiments. (**D**) The repression of PhoQ activity by high magnesium and MgrB. The activity of PhoQ was monitored with the GFP reporter system using the *E. coli ΔphoQΔmgrB* strain as described in Fig. 1E. Data are representative of three independent experiments. Each data point is shown with the calculated average and standard deviation from three biological replicates.

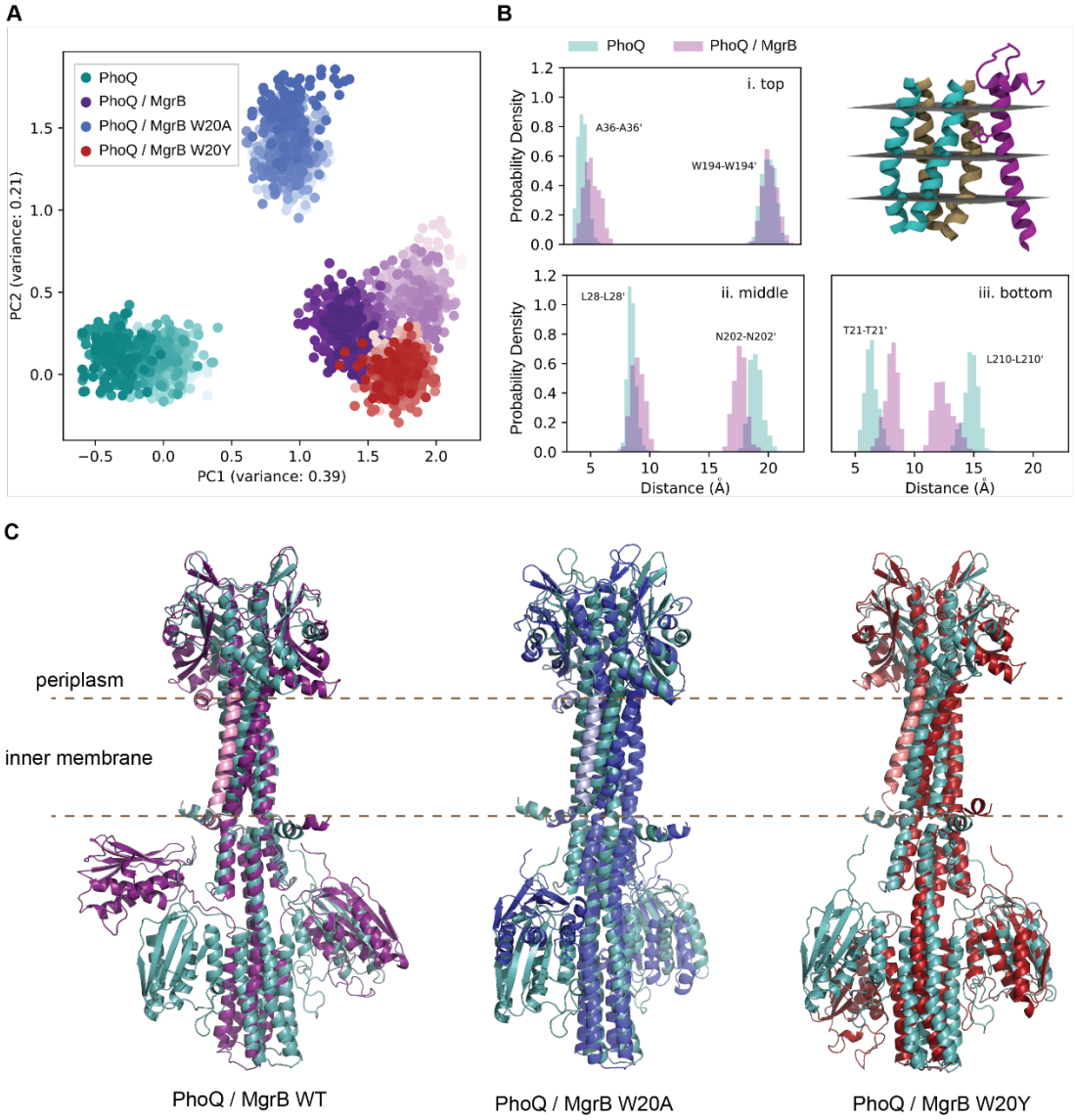

Fig. 4. Molecular dynamics simulations of PhoQ/MgrB complex models. (**A**) Projection of the molecular dynamics simulations into the eigenspace formed by the two first components of a Principal Component Analysis (PCA) of the transmembrane domain of PhoQ (residues 21 – 38 and 194 – 215). Each point corresponds to a conformation of the TM and is colored in shades of teal, purple, red and blue, for the simulations of PhoQ alone, and in complex with MgrB, MrgB W20Y and W20A, respectively. Lighter shades correspond to conformations sampled earlier in the simulation. (**B**) Distribution in distances between TM1 – TM1' (left) and TM2 – TM2' (right) at the top, middle, and bottom of PhoQ TM domain. (**C**) The overlay of the final conformations of PhoQ/MgrB complex models with PhoQ dimer. PhoQ structures are colored as in A. The MgrB wild-type, W20A, and W20Y variants are colored in pink, light blue, and light red, respectively.

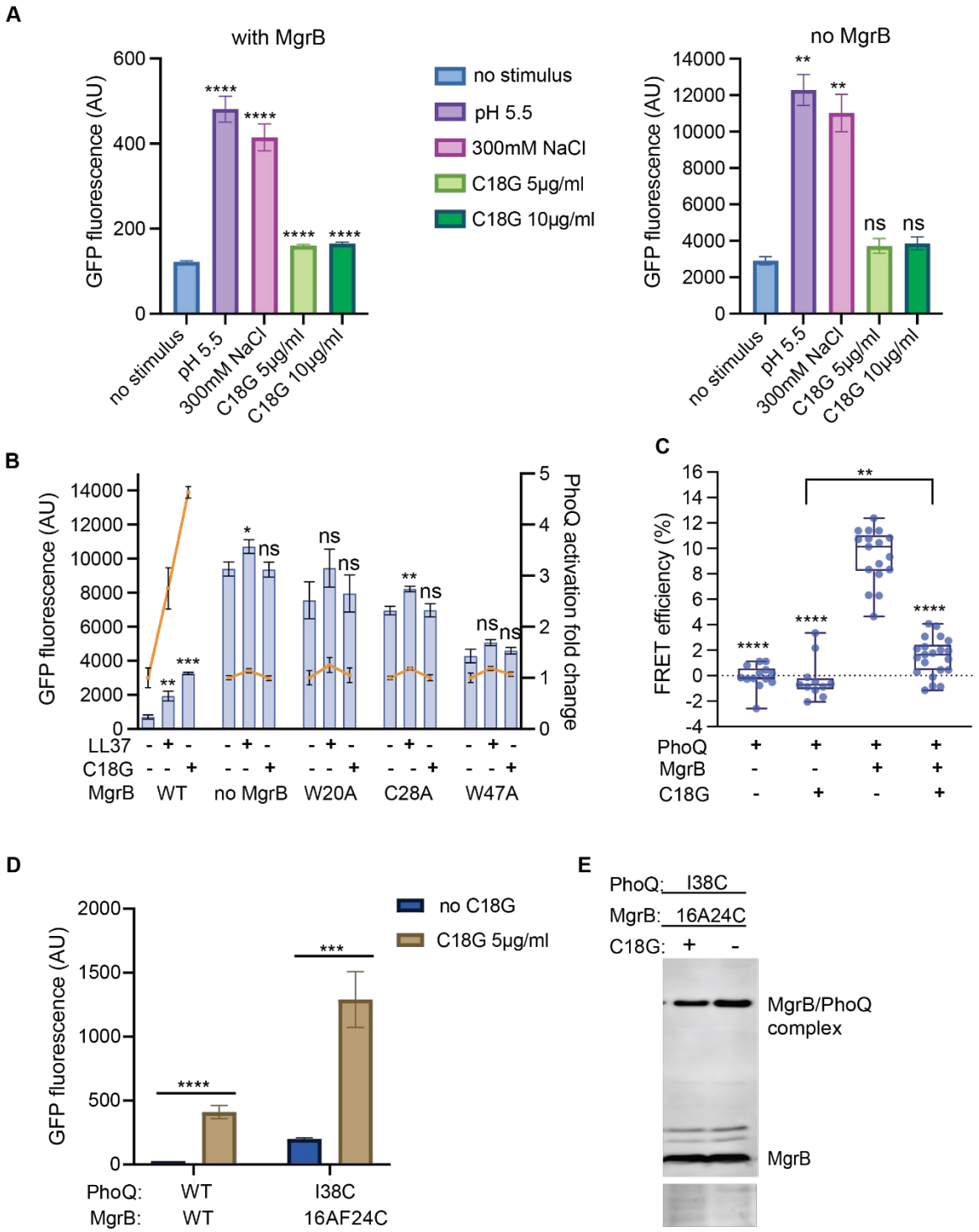

Fig. 5. The impact of MgrB on PhoQ sensing external stimuli. (**A**) The PhoQ activation in the presence or absence of MgrB under high magnesium conditions. *E. coli* MG1655 *ΔmgrB* strain harboring pBAD33 with (left panel) or without (right panel) *mgrB* gene, were induced with arabinose and grown in the presence of indicated stimuli in LB media supplemented with 10 mM magnesium. The activity of PhoQ was monitored using the GFP reporter as described in Fig. 1E. (**B**) The activation of PhoQ in the presence of antimicrobial peptides and MgrB under 1 mM

793 magnesium conditions. The orange lines indicate the fold change of PhoQ activity in the
794 presence of antimicrobial peptides. *E. coli* MG1655 *ΔmgrB* strain expressing MgrB variants were
795 grown in LB supplemented with 1 mM magnesium and antimicrobial peptides, LL37 (5 µg/ml) or
796 C18G (5 µg/ml) as indicated. The PhoQ activity was followed as in A. (**C**) The FRET measurements
797 of PhoQ-mNeonGreen and mCherry-MgrB *in vivo*. *E. coli* cells expressing PhoQ-mNeonGreen
798 and mCherry-MgrB from plasmids were grown to mid-log phase, then treated with or without
799 the antimicrobial peptide, C18G (10 µg/ml). The energy transfer from mNeonGreen to mCherry
800 was then measured for each condition. The strains expressing no FRET receptor (mCherry-MgrB)
801 serve as negative controls. (**D**) The activation of PhoQ variants in the presence of MgrB and
802 C18G (5 µg/ml). The growth and induction conditions for the PhoQ and MgrB variants were the
803 same as described before (Fig. 1F bottom). The PhoQ activity was monitored by measuring the
804 GFP reporter fluorescence. (**E**) Western blot analysis of PhoQ I38C MgrB 16A24C disulfide
805 crosslinking in the presence or absence of C18G (5 µg/ml). The crosslinking and Western blot
806 experiments were performed as described before (Fig. 1F top). The total protein stain of the
807 membrane serves as a loading control. Data are representative of three independent
808 experiments. Each data point in A-D is shown with the calculated average and standard
809 deviation from at least three independent experiments.
810

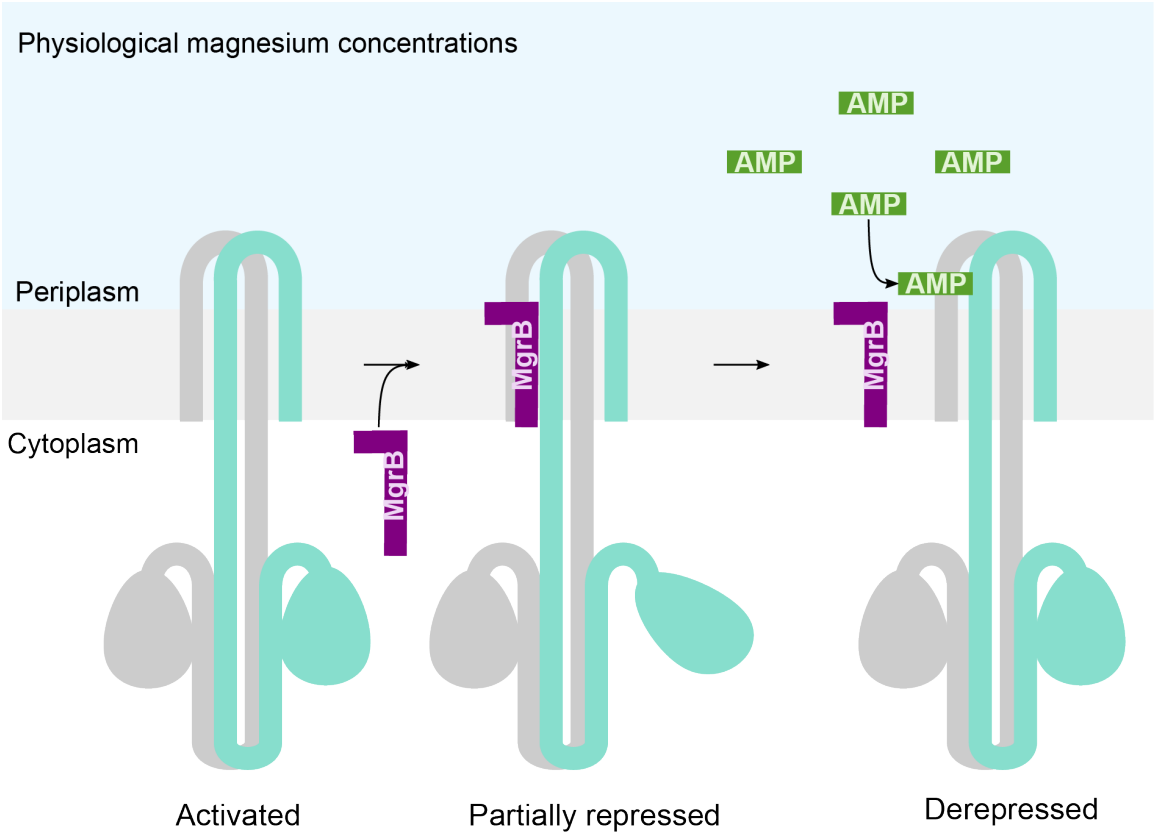

Fig. 6. The schematic representation of MgrB-mediated PhoQ activation by antimicrobial peptides. PhoQ is active under physiological magnesium conditions, inducing the expression of *mgrB*. The expressed MgrB binds to PhoQ, resulting in a partially repressed state. Antimicrobial peptides (AMPs) enter bacterial periplasm, bind to PhoQ, and cause MgrB to dissociate from PhoQ.

818 **Table 1.** The Cα - Cα distance of crosslinked residue pairs in the PhoQ/MgrB structural model.
819

Cα - Cα distance (Å)	W20-Y32	W20-L204	Q22-Y197	F24-I38
model 1	12.10	12.80	8.30	9.10
model 2	12.90	11.90	9.60	10.80
model 3	12.90	10.10	10.00	11.30
model 4	13.60	11.90	10.20	11.40
model 5	14.20	16.40	16.20	11.60

820
821

822 **Supporting Information**
823 **SI Materials and Methods**
824
825 **Cloning and plasmid construction**
826 *E. coli phoQ-his$_6$* gene was cloned into pET-Duet-1 vector at NcoI/BamHI restriction sites, and *E.*
827 *coli flag-mgrB* gene was cloned into pET-Duet-1 vector at NdeI/ EcoRV restriction sites. The
828 pEVOL-pBpF vector is a gift from Dr. Hans-Georg Koch (Freiburg, Germany). Mutations in *phoQ*
829 and *mgrB* were generated using the Q5 site-directed mutagenesis kit (New England BioLabs)
830 following the manufacturer's instruction. All constructs were verified by DNA sequencing.
831
832 **Purification of the crosslinked PhoQ-His/FLAG-MgrB complex**
833 A two-liter culture was prepared for the purification of the crosslinked PhoQ-His/FLAG-MgrB
834 complex. After UV crosslinking, cells were harvested, resuspended in the resuspension buffer
835 (20 mM Tris-HCl, pH 7.5, 300 mM NaCl, 0.1 mM PMSF), then lysed with LM10 microfluidizer at 4
836 °C. The lysate was centrifuged at 11,000 for 10 min to remove cell debris. The supernatant was
837 collected and centrifuged at 13,500 g for 2 hours to pellet the total membrane, which was then
838 dissolved in the resuspension buffer containing 1% (wt/vol) n-dodecyl-β-D-maltopyranoside
839 (DDM) with gentle shaking at 4 °C overnight. Insoluble fraction was spun down by centrifugation
840 at 21,000 g for 45 min. The supernatant was loaded onto a TALON column (Cytiva), which was
841 then washed three times with buffer containing 50 mM Tris-HCl, pH 8.0, 500 mM NaCl, 10%
842 glycerol, 10 mM imidazole, 0.1 mM PMSF and 0.03% DDM. The protein was eluted with elution
843 buffer containing 50 mM Tris-HCl, pH 8.0, 500 mM NaCl, 10% glycerol, 200 mM imidazole, 0.1
844 mM PMSF and 0.03% DDM, and concentrated to ~200 µL. The elution was then incubated with
845 anti-FLAG M2 magnetic beads (Sigma) at 4 °C overnight. The magnetic beads were washed with
846 Tris buffered saline, and then incubated with 3 X FLAG peptide solution (Sigma) at room
847 temperature for one hour to elute FLAG-tagged proteins. The supernatant was collected,
848 concentrated to ~50 µl, and analyzed using gel electrophoresis with a 7.5% tris-glycine
849 polyacrylamide gel.
850
851 **Protein verification with mass spectrometry**
852 Crosslinked and control bands were excised from SDS-PAGE gels and de-stained and sliced into
853 approx. 1mm^3 pieces. Proteins in the gel pieces were reduced (10 mM dithiothreitol, 56°C for 30
854 min), and alkylated (50 mM chloroacetamide, 30 min, RT, in the dark), prior to overnight
855 enzymatic hydrolysis with chymotrypsin (Promega, WI, USA) (0.1 µg of chymotrypsin per band in
856 50 mM ammonium bicarbonate buffer pH 7.4, 2 mM CaCl2) at 37°C. Following overnight
857 digestion, the peptides were collected and dried down via vacuum centrifugation (Concentrator
858 Plus, Eppendorf). Peptides were resuspended in 10 µl of HPLC loading buffer (3 % ACN + 0.1 %
859 trifluoroacetic acid) prior to LC-MS/MS analysis.
860
861 Chromatographic separation was performed on a Dionex U3000 nanoHPLC system (Thermo,
862 Germany) equipped with an Acclaim pepmap100 C18 column (2 µm particle size, 75 µm × 500
863 mm) coupled online to a QExactive Plus mass spectrometer (Thermo, Bremen). The separation
864 was performed over a 60-minute run: 5 % B for 3 minutes followed by linear gradients from 5 %
865 to 50 % B over 30 minutes, then 50 % to 90 % over 1 minute, and 10 minutes at 90 % B. Inter-run
866 equilibration was achieved by 15 minutes at 5 % B. Eluent A: 0.05 % formic acid (FA), eluent B:
867 80 % ACN + 0.04 % FA. A flow rate of 300 nl/min was used and 1 µl of sample was injected per
868 run. For crosslink samples a second injection of 6 µl was also performed. Full scan MS
869 acquisition was performed (300-1500 m/z, resolution 70,000, AGC target 3e6, max injection

870 time (IT) 100 ms) with subsequent data dependent MS/MS of the top 10 most intense ions via
871 HCD ion activation at NCE 27 (resolution 17,500, AGC target 1e5, isolation window 1.6 m/z, max
872 IT 50 ms); dynamic exclusion (20 s duration) and lock mass at 445.12003 m/z were enabled.
873
874 For protein identifications, the MS data files were processed with the Proteome Discoverer™
875 software suite (Ver. 2.5.0.400) (Thermo, Germany). Raw files were searched using the
876 SequestHT algorithmand Target Decoy PSM validator node, against a combined database that
877 included the proteins of interest (PhoQ-Histagged, the modified MgrB-pBpA incorporation
878 variants), the UniProt canonical proteins for *Escherichia coli* (strain K12) (accessed: 2022.03.10),
879 and common laboratory contaminants (cRAP list). Searches were performed with full
880 chymotrypsin specificity, and a maximum 3 missed cleavages. Precursor mass tolerance 10 ppm.
881 Fragment mass tolerance 0.02 Da. Fixed modification of carbamidomethyl (Cys), dynamic
882 modification oxidation (Met). Strict parsimony criteria were applied: Target FDR <1% was
883 applied, and at least one unique high confidence peptide was required for identification. For the
884 small protein MgrB, manual assessment of the peptide spectral matches was also performed.
885
886 **Acceptor photobleaching FRET data acquisition and analysis**
887 For each well, we acquired three or more sequences of images on isolated fields of view with
888 the following protocol: (a) 2 images in the acceptor channel; (b) 140 images in the donor
889 channel followed by (c) 16 seconds acceptor photobleaching (no image acquisition); (d) 50
890 images in the donor channel; and then (e) 2 images in the acceptor channel. FRET efficiency was
891 calculated as the increase of donor fluorescence signal upon acceptor photobleaching divided by
892 the total donor signal after acceptor photobleaching. In order to correct for the donor
893 photobleaching present during steps b to d, we performed linear fitting (RStudio) of the donor
894 fluorescence signal versus time for both pre- and postbleaching curves.
895
896

SI Figures and Tables

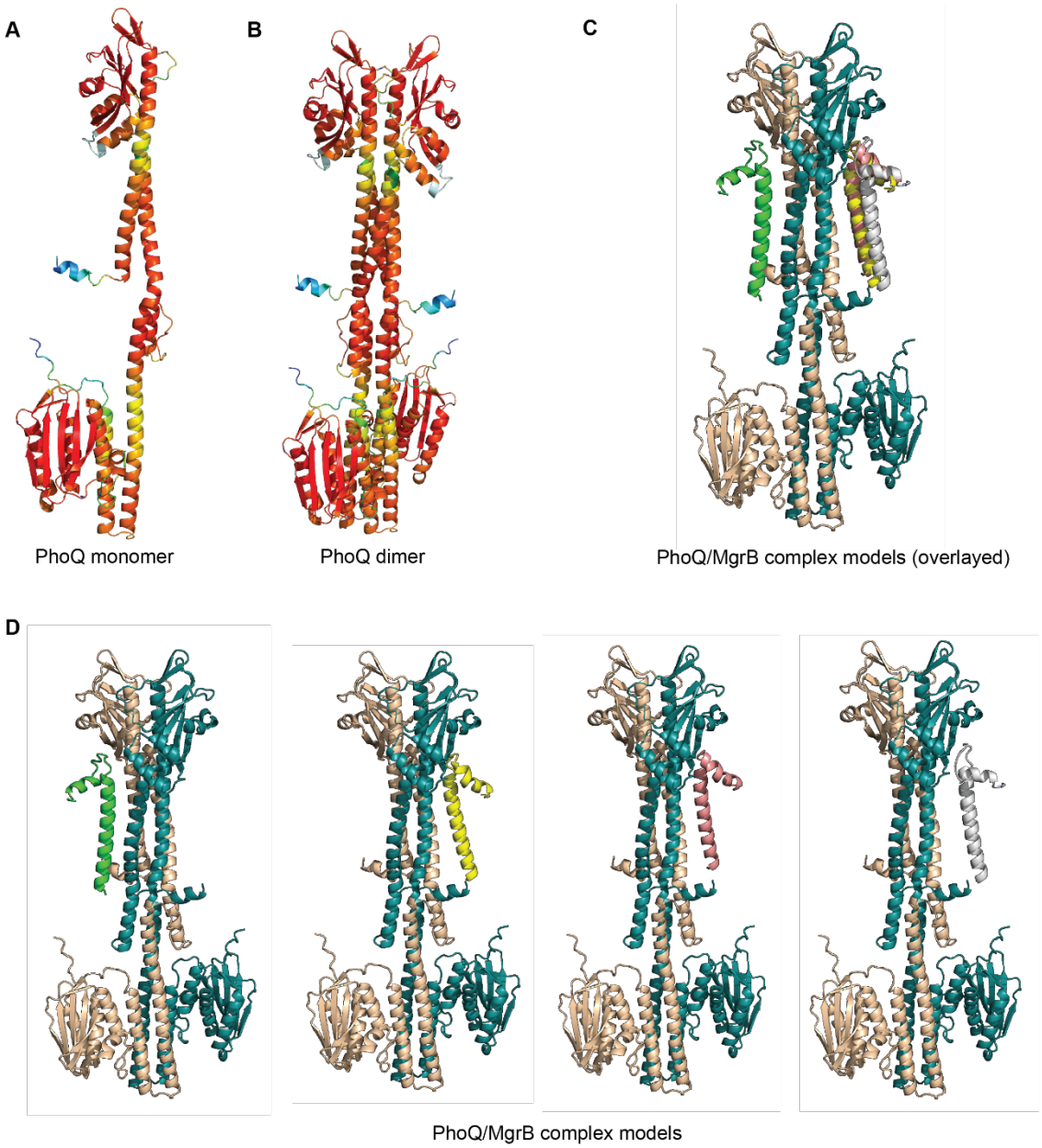

Fig. S1. Structural models predicted by Alphafold2. (**A-B**) The predicted PhoQ monomer and dimer are colored according to the pLDDT score to show the regions with lower prediction confidence. Red indicates highest confidence and blue indicates lowest confidence. The four predicted PhoQ/MgrB complex models ranked from two to five by Alphafold2. Models are shown with a PhoQ dimer (colored in wheat and deep teal) and four MgrB molecules overlayed (**C**) or separated (**D**) in green, yellow, pink and grey ranked from 2 to 5, respectively. All structural figures were prepared using PyMOL unless otherwise stated.

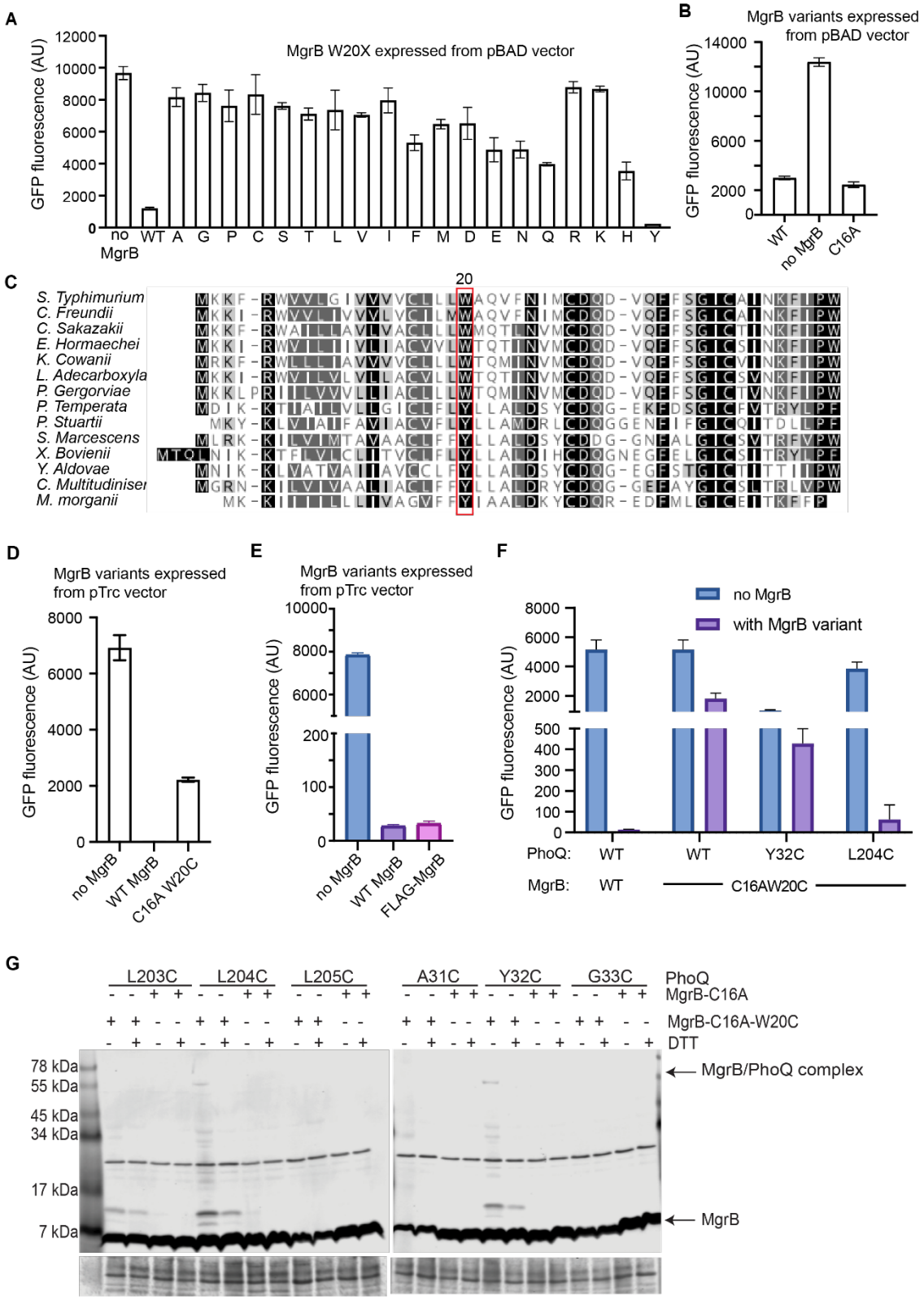

Fig. S2. The function of MgrB variants and the crosslinking with PhoQ from MgrB position 20. The activity analysis of MgrB W20 variants (**A**) and MgrB C16A (**B**) using the reporter plasmid

914 pUA66 P_{mgtLA}-*gfp*. The *E. coli ΔmgrB* strain harboring the reporter plasmid and the pBAD plasmid
915 with *mgrB* variants were grown to the early log phase in LB media supplemented with 0.008%
916 arabinose. GFP fluorescence in cells was then measured by flow cytometry. (**C**) Sequence
917 alignment of MgrB homologs from fourteen bacterial species. The conservation of the amino
918 acid at position 20 (*E. coli* numbering) is highlighted with a red rectangle. (**D**) The functional
919 assay of MgrB variants expressed from pTrc99A vector. The pUA66 P_{mgtLA}-*gfp*, pBAD33 *phoQ*,
920 and pTrc99A plasmid with flag tagged *mgrB* variants, were transformed into *E.*
921 *coli ΔphoQΔmgrB* cells. The resulting transformants were grown overnight at 37 °C in LB
922 medium supplemented with 10 mM MgSO4, then diluted 1:100 to fresh LB medium
923 supplemented with 1 mM MgSO4, 0.008% arabinose, 10 µM IPTG, and antibiotics when
924 appropriate. The cultures were grown at 37 °C with vigorous shaking till the early log phase. The
925 GFP fluorescence of cells was then monitored by flow cytometry. (**E**) The functional assay of
926 MgrB and Flag-MgrB expressed from pTrc99A vector. The pUA66 P_{mgtLA}-*gfp* and pTrc99A plasmid
927 with *mgrB* or *flag-mgrB*, were transformed into *E. coli ΔmgrB* cells. The resulting transformants
928 were grown overnight at 37 °C in LB medium supplemented with 10 mM MgSO4, then diluted
929 1:100 to fresh LB medium supplemented with 1 mM MgSO4, 10 µM IPTG, and antibiotics when
930 appropriate. The cultures were grown at 37 °C with vigorous shaking till the early log phase. The
931 GFP fluorescence of cells was then monitored by flow cytometry. (**F**) The functional assay of the
932 indicated PhoQ and MgrB variants using the same protocol as in D. (**G**) Western blot analysis
933 of *E. coli* membrane extracts after disulfide crosslinking. The indicated PhoQ and FLAG-tagged
934 MgrB variants were expressed in *E. coli*, followed by Cu-phenanthroline catalyzed disulfide
935 crosslinking (details in Materials and Methods). The total protein stain of the PVDF membranes
936 serves as loading controls. Data are representative of at least three independent experiments. In
937 A, B, D, E and F, each data point is shown with the calculated average and standard deviation
938 from three independent biological replicates.
939
940

941

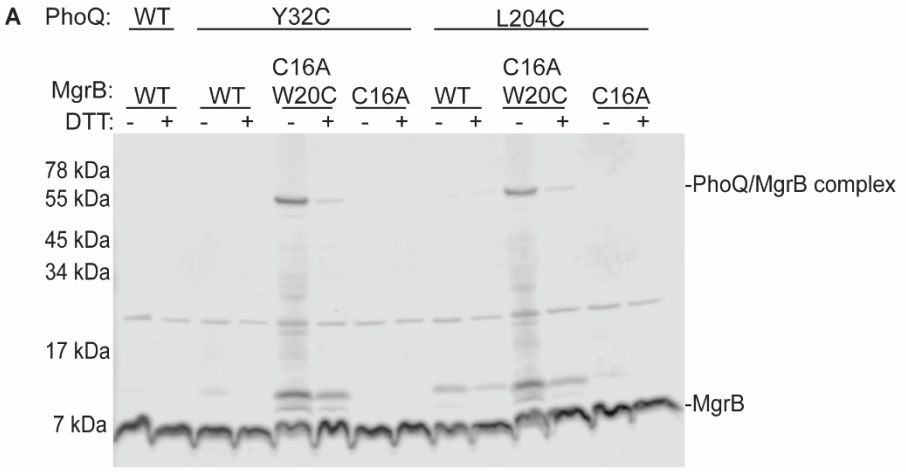
A
PhoQ: WT Y32C L204C
MgrB: WT WT C16A W20C C16A WT C16A W20C C16A
DTT: - + - + - + - + - + - + - +
78 kDa
55 kDa
45 kDa
34 kDa
17 kDa
7 kDa
-PhoQ/MgrB complex
-MgrB

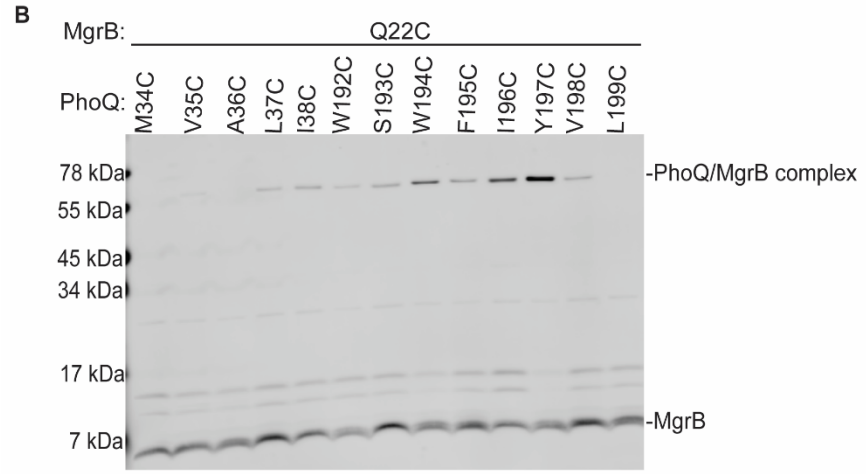
B
MgrB: Q22C
PhoQ: M34C V35C A36C L37C I38C W192C S193C W194C F195C I196C Y197C V198C L199C
78 kDa
55 kDa
45 kDa
34 kDa
17 kDa
7 kDa
-PhoQ/MgrB complex
-MgrB

942

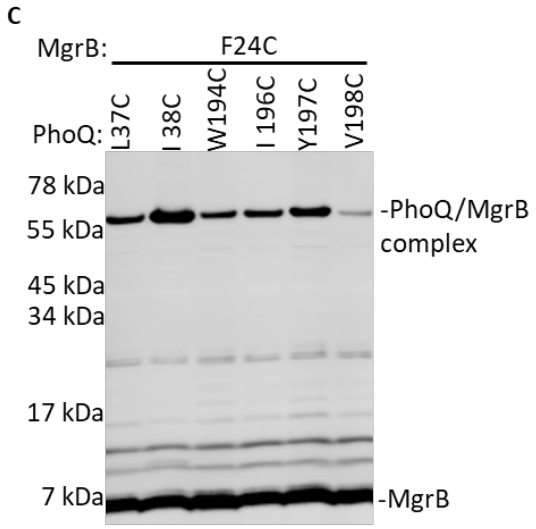
C
MgrB: F24C
PhoQ: L37C I 38C W194C I 196C Y197C V198C
78 kDa
55 kDa
45 kDa
34 kDa
17 kDa
7 kDa
-PhoQ/MgrB complex
-MgrB

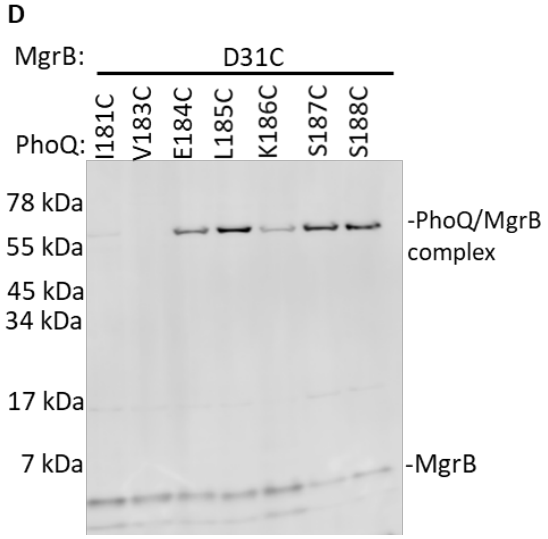
D
MgrB: D31C
PhoQ: I181C V183C E184C L185C K186C S187C S188C
78 kDa
55 kDa
45 kDa
34 kDa
17 kDa
7 kDa
-PhoQ/MgrB complex
-MgrB

943

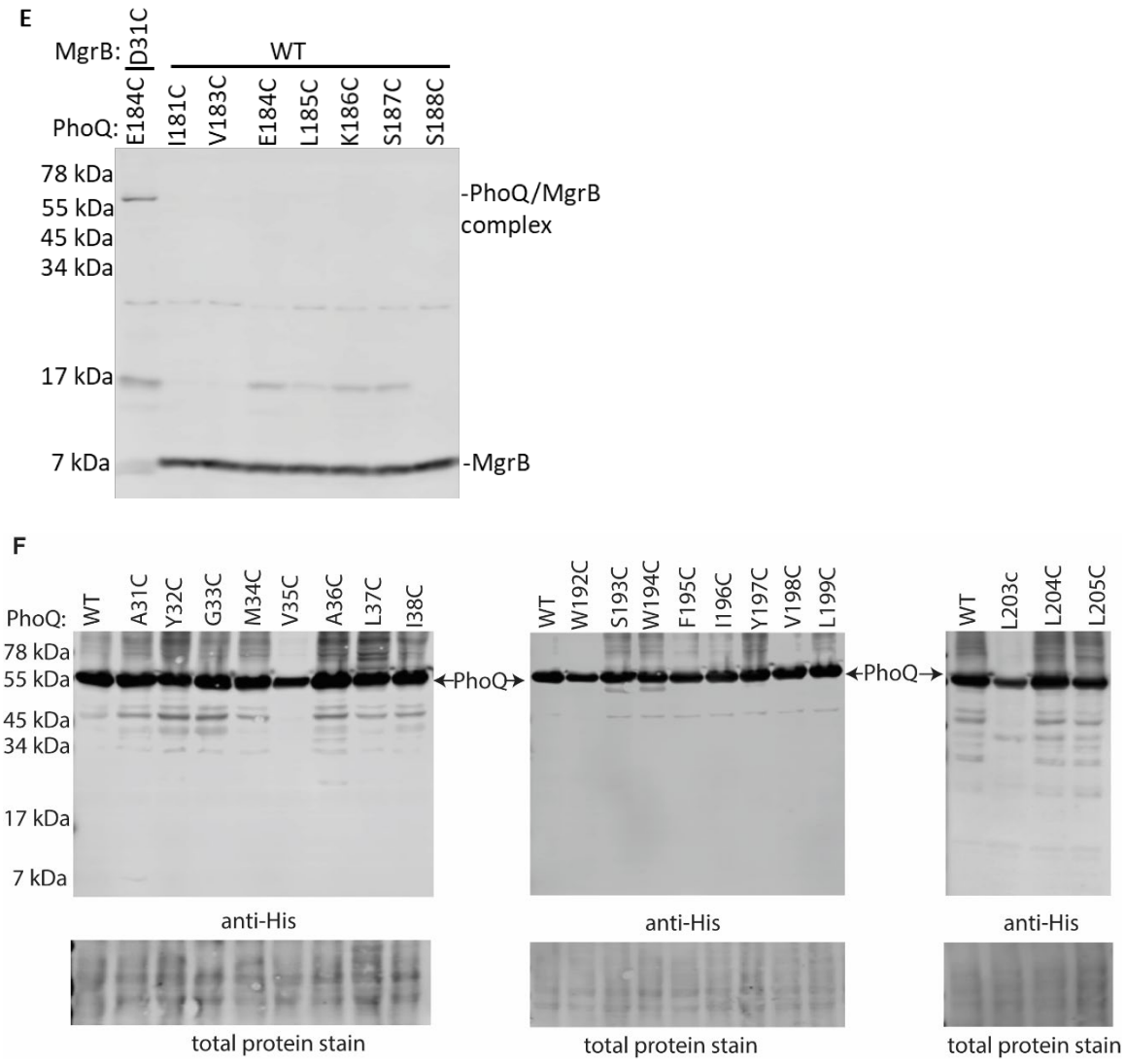

Fig. S3. The full Western blot results of the figures in the main text. (**A**) is the full blot of Fig. 1D. (**B**) is the full blot of Fig. 1E. (**C**) is the full blot of Fig. 1F. (**D, E**) are the full blots of Fig. 2B. Data are representative of at least three independent experiments. (**F**) Western blot analysis of the expression level of PhoQ variants. The indicated PhoQ-His variants were expressed in *E. coli* by inducing with 0.008% arabinose. Cells were harvested in the mid log phase and the total membrane was extracted for the western blot analysis. The total protein stain of the PVDF membranes serves as a loading control. Data are representative of two independent experiments.

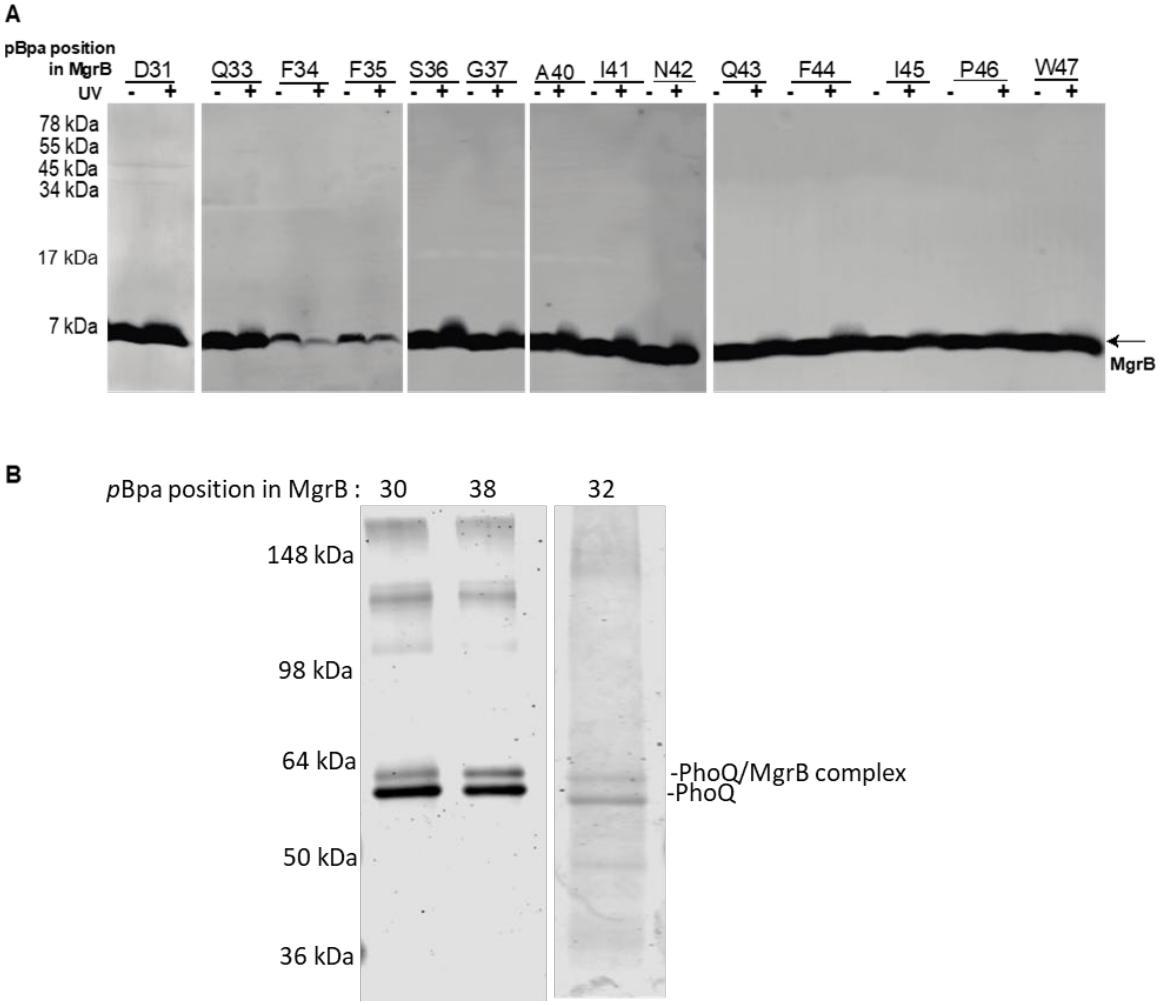

957
958 **Fig. S4. Mapping the binding interface of MgrB on PhoQ by using site-specific UV crosslinking**
959 **in *vivo*.** (**A**) *E. coli* BL21 DE3 cells expressing PhoQ-His$_6$, FLAG-MgrB or *p*Bpa-containing FLAG-
960 MgrB variants were irradiated with or without UV light. The cells were lysed in SDS sample
961 buffer. Proteins were separated on 7.5% tris-glycine polyacrylamide gels and transfer to PVDF
962 membranes. FLAG tagged proteins were detected with an anti-FLAG primary antibody and an
963 IRDye 800CW-conjugated secondary antibody. Data are representative of three independent
964 experiments. (**B**) Purification of PhoQ-His/FLAG-MgrB crosslinked complex. Elution from a two-
965 step affinity purification was separated on 7.5% tris-glycine gels. The protein bands in the gel
966 were visualized with the ready-blue protein stain. Data are representative of two independent
967 experiments.
968

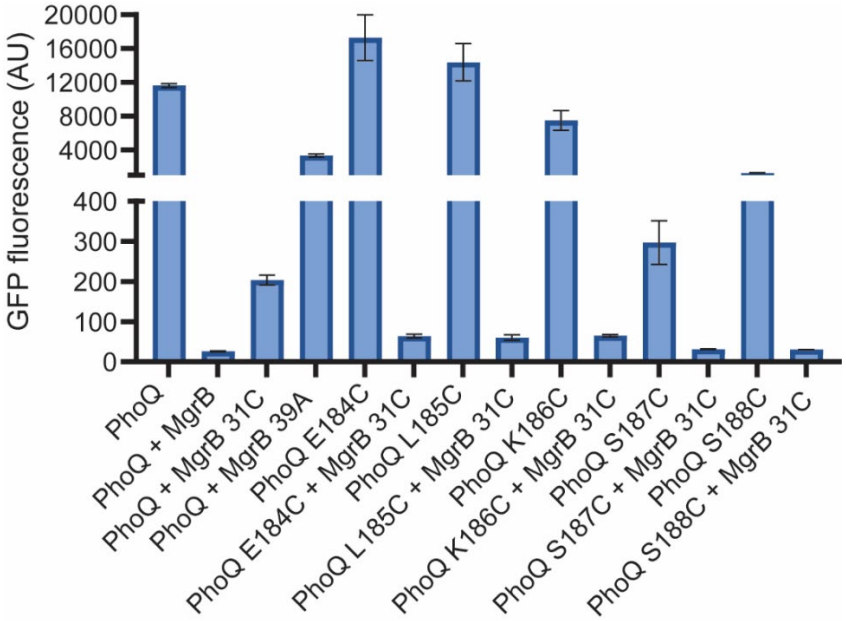

969
970 **Fig. S5. The functional assay of PhoQ variants with or without MgrB.** *E. coli* MG1655
971 *ΔphoQΔmgrB* cells harboring pBAD33 *phoQ* variants, the GFP reporter plasmid pUA66 P_{mgtA}-*gfp*,
972 pTrc99A with or without *mgrB* variants were grown in LB supplemented with 0.008% arabinose
973 and 10 μM IPTG till the early-log phase. The GFP fluorescence of the cells was measured with
974 flow cytometry. Each data point is shown with the calculated average and standard deviation
975 from three biological replicates. The results are the representative of at least three independent
976 experiments.
977

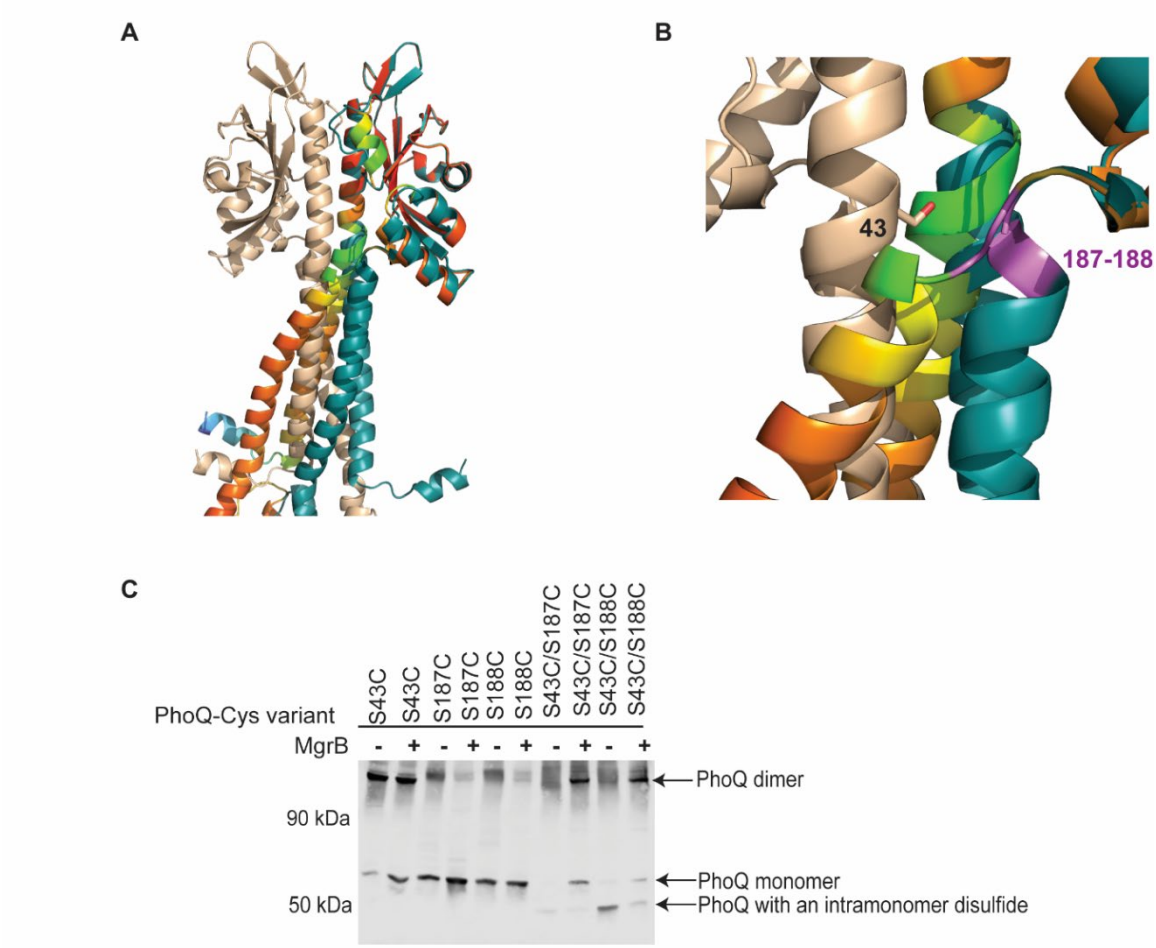

Fig. S6. The conformational change of PhoQ linker region in the presence of MgrB. (**A**) The structural superimposition of the periplasmic and TM domains of the PhoQ dimer (wheat and deep teal) and monomer (pLDDT) is shown. The periplasmic domain was used for structural alignment in Pymol. (**B**) Zoom in view of the linker region of PhoQ. Residue 43 is shown in ball-and-stick. Residues 187 and 188 are colored in purple in both monomer and dimer structures. (**C**) Western blot analysis of disulfide crosslinking within the PhoQ molecule in the presence or absence of MgrB. The crosslinked PhoQ species was detected with an anti-His antibody. Data are representative of at least three independent experiments.

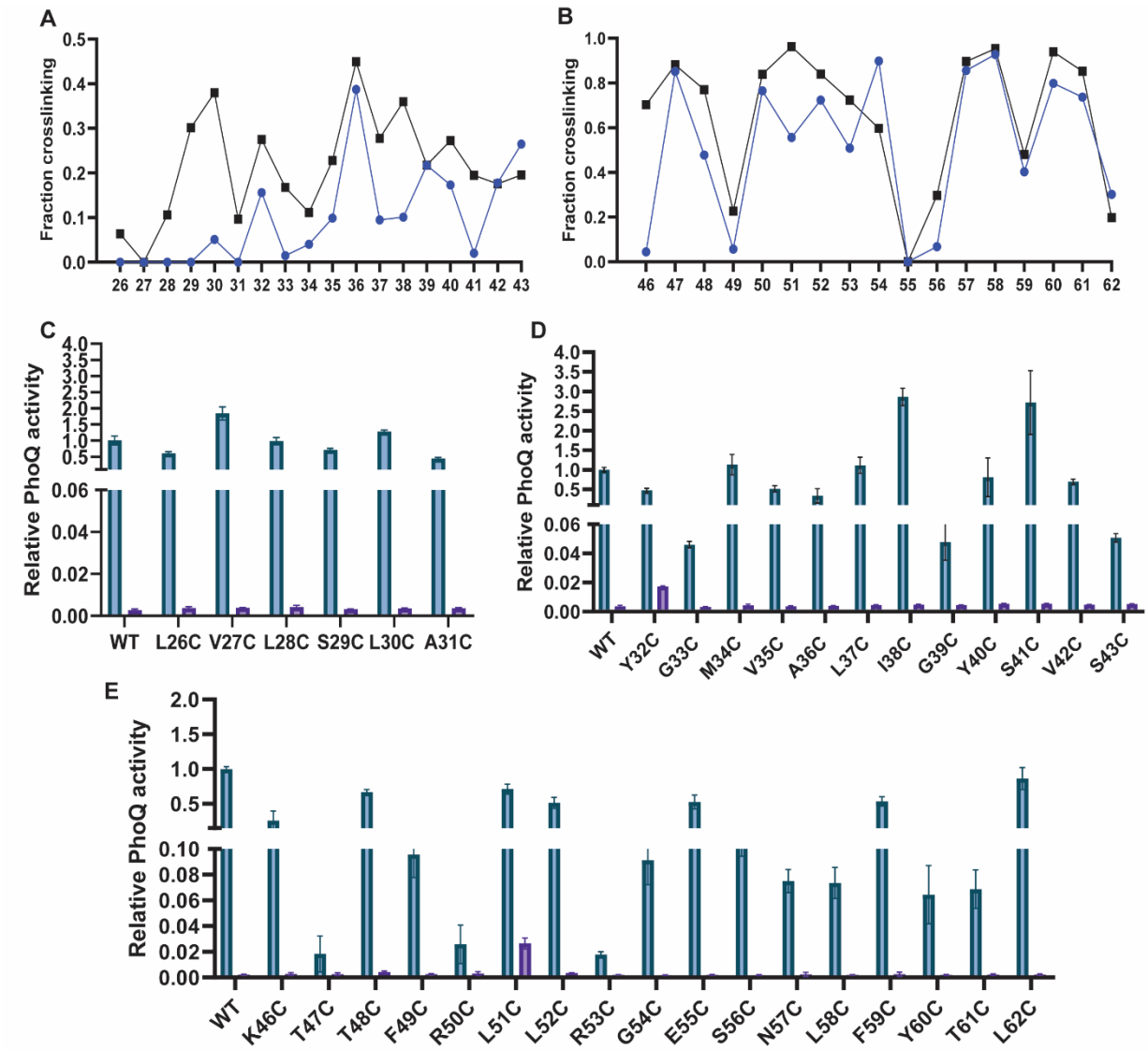

Fig. S7. **PhoQ_Cys variants in the presence or absence of MgrB.** (**A-B**) Quantification of the disulfide crosslinking efficiency of PhoQ_Cys variants in the presence (blue curve) and absence (black curve) of MgrB. The PhoQ dimer and monomer bands in Fig. 4C were quantified with ImageJ. The fraction of crosslinked dimer was calculated using the formula: crosslinking fraction = dimer / (dimer + monomer). (**C-E**) Functional assays of PhoQ_Cys variants with (blue) and without (purple) MgrB. *E. coli ΔphoQΔmgrB* cells harboring pUA66 P_{mgtA}-*gfp*, pBAD33 *phoQ* variants, and pTrc99A empty or pTrc99A *mgrB* were grown overnight at 37 °C in LB medium supplemented with 10 mM $MgSO_4$. Cultures were then diluted 1:100 to fresh LB medium supplemented with 1 mM $MgSO_4$, 0.008% arabinose and 10 μM IPTG, and grown at 37 °C with vigorous shaking till the early log phase (OD=0.4-0.5). The fluorescence of cells was monitored with flow cytometry and normalized to the PhoQ wild type. Each data point in C, D and E is shown with the calculated average and standard deviation from three biological replicates. The results are the representative of three independent experiments.

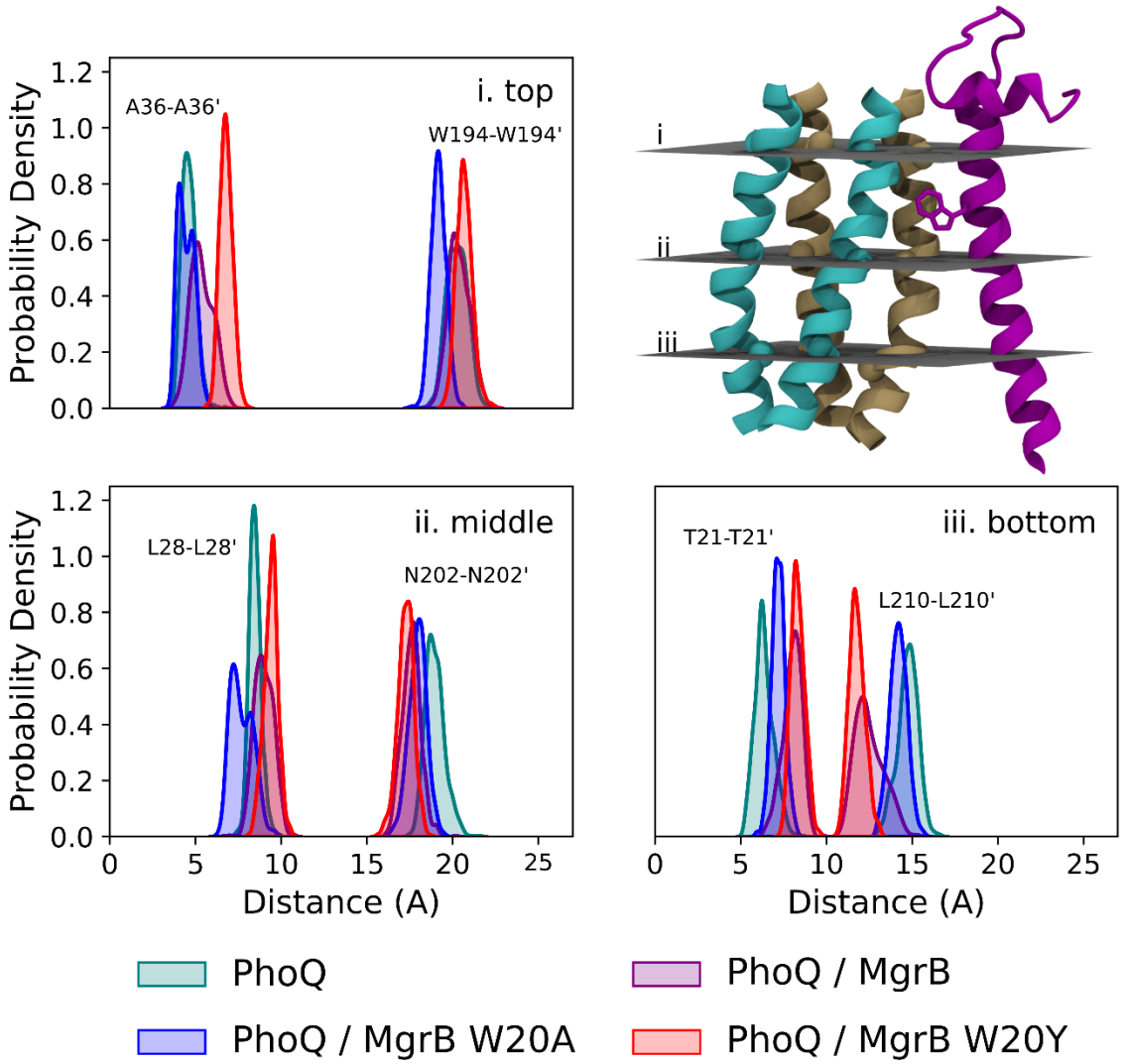

Fig. S8. MD simulations of PhoQ/MgrB complex models. Distribution in distances between TM1 – TM1' (left) and TM2 – TM2' (right) at the top, middle, and bottom of PhoQ TM domain.

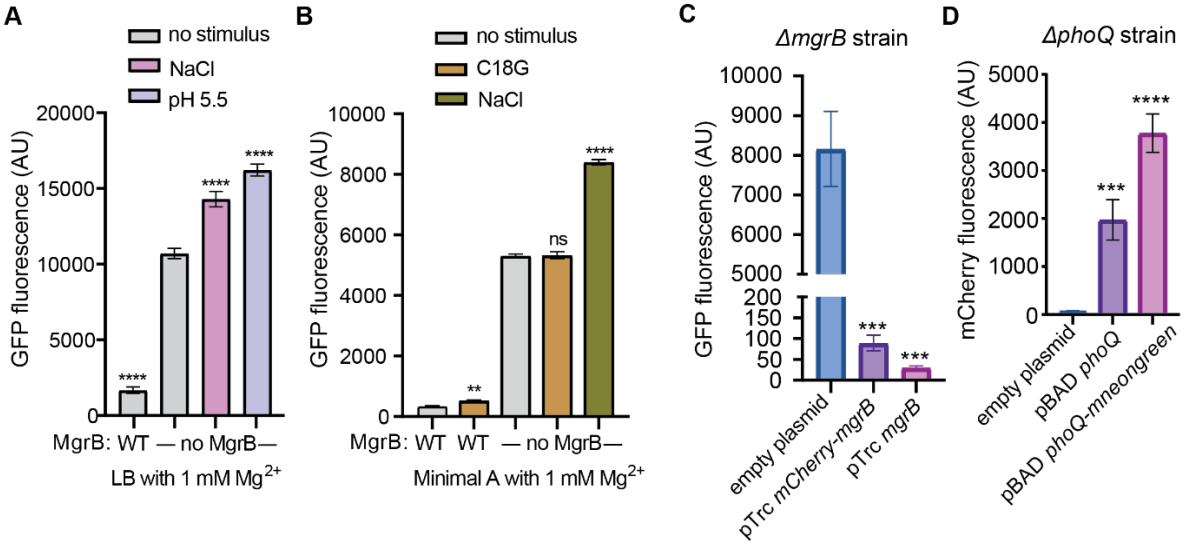

Fig. S9. The functional assays with fluorescent reporters. PhoQ activity was monitored with a GFP reporter plasmid (pUA66 P_{mgtLA}-*gfp*) with or without MgrB in LB (**A**) and in minimal A medium (**B**) supplemented with 1 mM magnesium. Breifly, *E. coli ΔmgrB* strain harboring the GFP reporter plasmid and a pBAD plasmid with or without the wild-type mgrB gene, was grown in the presence of the indicated PhoQ stimuli to early log phase. The GFP fluorescence of cells was then measured by flow cytometry. Data are representative of at least three independent experiments. The function of fusion proteins mCherry-MgrB (**C**) and PhoQ-mneonGreen (**D**) were anlalyzed with the GFP report and a mCherry reporter (pUA66 P_{mgtLA}-*mcherry*). Indicated deletion strains were complemented with a plasmid harboring the gene of indicated fusion proteins. The expression of the fusion protein was induced with 10 μM IPTG and 0.008% arabinose for the pTrc and pBAD plasmids, respectively. Cells were grown to early log phase and the fluorescence of cells was measured by flow cytometry. Cells transformed with empty plasmids and plasmids harboring the corresponding wild-type genes were used as negative and positive controls, respectively. Data are representative of two independent experiments.

1024 **Table S1. List of strains used in this study.**

1025

Strain	Genotype	Source or Reference
JingY11	MG1655	*E. coli* Genetic Stock Center, CGSC# 7740
lptD4213	F-, *lptD4213*, *galK2*(Oc), λ^-, *IN(rrnD-rrnE)1*, *rpsL200*(strR), *rph-1*	Yale Coli Genetic Stock Center
E. coli BL21(DE3)	BL21(DE3)	New England Biolabs
JingY34	MG1655 Δ*mgrB::FRT*	[1]
JingY90	MG1655 Δ*phoQ::FRT* Δ*mgrB::FRT*	[1]

1026

1027

1028 **Table S2. List of plasmids used in this study.**

1029

Plasmid	Genotype	Source or Reference
pJY1	pBAD33 *phoQ-(his)$_6$*	This study
pJY31	pBAD33RBS	[2]
pJY151	pBAD33RBS *mgrB*	[1]
pOB2	pTrc99A *mcherry*	[1]
pJY569	pTrc99A *mcherry-mgrB*	[1]
pJY573	pBAD33RBS *phoQ-mneongreen*	[1]
pJY317	pTrc99A *flag-mgrB*	This study
pJS1	pET-Duet-1 EC *phoQ-his$_6$*, *flag-mgrB*	This study
pEVOL	pEVOL-pBpF	A gift from Dr. Hans-Georg Koch
pLS1	pBAD33RBS *phoQ L26C*	This study
pLS2	pBAD33RBS *phoQ V27C*	This study
pLS3	pBAD33RBS *phoQ L28C*	This study
pLS4	pBAD33RBS *phoQ S29C*	This study
pLS5	pBAD33RBS *phoQ L30C*	This study
pLS6	pBAD33RBS *phoQ A31C*	This study
pLS7	pBAD33RBS *phoQ Y32C*	This study
pLS8	pBAD33RBS *phoQ G33C*	This study
pLS9	pBAD33RBS *phoQ M34C*	This study
pLS10	pBAD33RBS *phoQ V35C*	This study
pLS11	pBAD33RBS *phoQ A36C*	This study
pLS12	pBAD33RBS *phoQ L37C*	This study
pLS13	pBAD33RBS *phoQ I38C*	This study

pLS14	pBAD33RBS *phoQ G39C*	This study
pLS15	pBAD33RBS *phoQ Y40C*	This study
pLS16	pBAD33RBS *phoQ S41C*	This study
pLS17	pBAD33RBS *phoQ V42C*	This study
pLS18	pBAD33RBS *phoQ S43C*	This study
pLS19	pBAD33RBS *phoQ F44C*	This study
pJS4	pBAD33RBS *phoQ K46C*	This study
pJS5	pBAD33RBS *phoQ T47C*	This study
pJS6	pBAD33RBS *phoQ T48C*	This study
pJS7	pBAD33RBS *phoQ F49C*	This study
pJS8	pBAD33RBS *phoQ R50C*	This study
pJS9	pBAD33RBS *phoQ L51C*	This study
pJS10	pBAD33RBS *phoQ L52C*	This study
pJS11	pBAD33RBS *phoQ R53C*	This study
pJS12	pBAD33RBS *phoQ G54C*	This study
pJS13	pBAD33RBS *phoQ E55C*	This study
pJS14	pBAD33RBS *phoQ S56C*	This study
pJS15	pBAD33RBS *phoQ N57C*	This study
pJS16	pBAD33RBS *phoQ L58C*	This study
pJS17	pBAD33RBS *phoQ F59C*	This study
pJS18	pBAD33RBS *phoQ Y60C*	This study
pJS19	pBAD33RBS *phoQ T61C*	This study
pJS20	pBAD33RBS *phoQ L62C*	This study
pJS21	pBAD33RBS *phoQ D179C*	This study
pJS22	pBAD33RBS *phoQ T181C*	This study

pJS23	pBAD33RBS *phoQ I183C*	This study
pJS24	pBAD33RBS *phoQ E184C*	This study
pJS25	pBAD33RBS *phoQ L185C*	This study
pJS26	pBAD33RBS *phoQ K186C*	This study
pLS20	pBAD33RBS *phoQ S187C*	This study
pLS21	pBAD33RBS *phoQ S188C*	This study
pLS22	pBAD33RBS *phoQ S43C-S187C*	This study
pLS23	pBAD33RBS *phoQ S43C-S188C*	This study
pCK1	pBAD33RBS *phoQ S193C*	This study
pCK2	pBAD33RBS *phoQ W194C*	This study
pCK3	pBAD33RBS *phoQ F195C*	This study
pCK4	pBAD33RBS *phoQ I196C*	This study
pCK5	pBAD33RBS *phoQ Y197C*	This study
pCK6	pBAD33RBS *phoQ V198C*	This study
pCK7	pBAD33RBS *phoQ L199C*	This study
pCK8	pBAD33RBS *phoQ S200C*	This study
pCK9	pBAD33RBS *phoQ N202C*	This study
pCK10	pBAD33RBS *phoQ L203C*	This study
pCK11	pBAD33RBS *phoQ L204C*	This study
pCK12	pBAD33RBS *phoQ L205C*	This study
pCK13	pBAD33RBS *phoQ V206C*	This study
pCK14	pBAD33RBS *phoQ I207C*	This study
pCK15	pBAD33RBS *phoQ L209C*	This study
pCK16	pBAD33RBS *phoQ L210C*	This study
pCK17	pBAD33RBS *phoQ W211C*	This study

pCK18	pBAD33RBS *phoQ V212C*	This study
pCK19	pBAD33RBS *phoQ A213C*	This study
pCK20	pTrc99A *mgrB C16A*	This study
pCK21	pTrc99A *mgrB C16A W20C*	This study
pCK22	pTrc99A *mgrB C16A Q22C*	This study
pCK23	pTrc99A *mgrB C16A F24C*	This study
pJS27	pTrc99A *mgrB D31C*	This study
pJY268	pBAD33RBS *mgrB W20A*	This study
pJY156	pBAD33RBS *mgrB C28A*	This study
pJS51	pET-Duet-1 *mgrB N25-TAG*	This study
pJS52	pET-Duet-1 *mgrB M26-TAG*	This study
pJS53	pET-Duet-1 *mgrB M27-TAG*	This study
pJS54	pET-Duet-1 *mgrB D29-TAG*	This study
pJS55	pET-Duet-1 *mgrB Q30-TAG*	This study
pJS56	pET-Duet-1 *mgrB D31-TAG*	This study
pJS57	pET-Duet-1 *mgrB V32-TAG*	This study
pJS58	pET-Duet-1 *mgrB Q33-TAG*	This study
pJS59	pET-Duet-1 *mgrB F34-TAG*	This study
pJS60	pET-Duet-1 *mgrB F35-TAG*	This study
pJS61	pET-Duet-1 *mgrB S36-TAG*	This study
pJS62	pET-Duet-1 *mgrB G37-TAG*	This study
pJS63	pET-Duet-1 *mgrB I38-TAG*	This study
pJS64	pET-Duet-1 *mgrB A40-TAG*	This study
pJS65	pET-Duet-1 *mgrB I41-TAG*	This study
pJS66	pET-Duet-1 *mgrB N42-TAG*	This study

pJS67	pET-Duet-1 *mgrB Q43-TAG*	This study
pJS68	pET-Duet-1 *mgrB F44-TAG*	This study
pJS69	pET-Duet-1 *mgrB I45-TAG*	This study
pJS70	pET-Duet-1 *mgrB P46-TAG*	This study
pJS71	pET-Duet-1 *mgrB W47-TAG*	This study

1030
1031

1032 **Table S3. List of primers used in this study.**

1033

Primer	Sequence (5' -> 3')
pBAD33RBS *phoQ L26C* fw	AGCGGTAGTAtgcGTGCTTTCGCTTGC
pBAD33RBS *phoQ L26C* rv	GCCGTTGCCAACAGAAAA
pBAD33RBS *phoQ V27C* fw	GGTAGTACTGtgcCTTTCGCTTGCCTACGGAATG
pBAD33RBS *phoQ V27C* rv	GCTGCCGTTGCCAACAGA
pBAD33RBS *phoQ L28C* fw	AGTACTGGTGtgcTCGCTTGCCTACGGAATGG
pBAD33RBS *phoQ L28C* rv	ACCGCTGCCGTTGCCAAC
pBAD33RBS *phoQ S29C* fw	ACTGGTGCTTtgcCTTGCCTACGGAATGG
pBAD33RBS *phoQ S29C* rv	ACTACCGCTGCCGTTGCC
pBAD33RBS *phoQ L30C* fw	GGTGCTTTCGtgcGCCTACGGAATGG
pBAD33RBS *phoQ L30C* rv	AGTACTACCGCTGCCGTT
pBAD33RBS *phoQ A31C* fw	GCTTTCGCTTtgcTACGGAATGGTCG
pBAD33RBS *phoQ A31C* rv	ACCAGTACTACCGCTGCC
pBAD33RBS *phoQ Y32C* fw	TTCGCTTGCCtgcGGAATGGTCG
pBAD33RBS *phoQ Y32C* rv	AGCACCAGTACTACCGCTG
pBAD33RBS *phoQ G33C* fw	GCTTGCCTACtgcATGGTCGCGC
pBAD33RBS *phoQ G33C* rv	GAAAGCACCAGTACTACCG
pBAD33RBS *phoQ M34C* fw	TGCCTACGGAtgcGTCGCGCTGATC
pBAD33RBS *phoQ M34C* rv	AGCGAAAGCACCAGTACT
pBAD33RBS *phoQ V35C* fw	CTACGGAATGtgcGCGCTGATCG
pBAD33RBS *phoQ V35C* rv	GCAAGCGAAAGCACCAGT
pBAD33RBS *phoQ A36C* fw	CGGAATGGTCtgcCTGATCGGTTATAGCG
pBAD33RBS *phoQ A36C* rv	TAGGCAAGCGAAAGCACC
pBAD33RBS *phoQ L37C* fw	AATGGTCGCGtgcATCGGTTATAGCGTCAGTTTC
pBAD33RBS *phoQ L37C* rv	CCGTAGGCAAGCGAAAGC
pBAD33RBS *phoQ I38C* fw	GGTCGCGCTGtgcGGTTATAGCG
pBAD33RBS *phoQ I38C* rv	ATTCCGTAGGCAAGCGAAAG
pBAD33RBS *phoQ G39C* fw	CGCGCTGATCtgcTATAGCGTCAG 66C
pBAD33RBS *phoQ G39C* rv	ACCATTCCGTAGGCAAGC
pBAD33RBS *phoQ Y40C* fw	GCTGATAGGTtgcAGCGTCAGTTTC
pBAD33RBS *phoQ Y40C* rv	GCGACCATTCCGTAGGCA
pBAD33RBS *phoQ S41C* fw	GATCGGTTATtgcGTCAGTTTCGATAAAAC
pBAD33RBS *phoQ S41C* rv	AGCGCGACCATTCCGTAG
pBAD33RBS *phoQ V42C* fw	CGGTTATAGCtgcAGTTTCGATAAAACTACGTTTC
pBAD33RBS *phoQ V42C* rv	ATCAGCGCGACCATTCCG
pBAD33RBS *phoQ S43C* fw	TTATAGCGTCtgcTTCGATAAAACTACGTTTC
pBAD33RBS *phoQ S43C* rv	CCGATCAGCGCGACCATT
pBAD33RBS *phoQ F44C* fw	TAGCGTCAGTtgcGATAAAACTACG

pBAD33RBS *phoQ F44C* rv	TAACCGATCAGCGCGACC
pBAD33RBS *phoQ K46C* fw	CAGTTTCGATtgcACTACGTTTCGG
pBAD33RBS *phoQ K46C* rv	ACGCTATAACCGATCAGC
pBAD33RBS *phoQ T47C* fw	TTTCGATAAAtgcACGTTTCGGCTGTTAC
pBAD33RBS *phoQ T47C* rv	CTGACGCTATAACCGATC
pBAD33RBS *phoQ T48C* fw	CGATAAAACTtgcTTTCGGCTGTTACGTG
pBAD33RBS *phoQ T48C* rv	AAACTGACGCTATAACCG
pBAD33RBS *phoQ F49C* fw	TAAAACTACGtgcCGGCTGTTAC
pBAD33RBS *phoQ F49C* rv	TCGAAACTGACGCTATAAC
pBAD33RBS *phoQ R50C* fw	AACTACGTTTtgcCTGTTACGTG
pBAD33RBS *phoQ R50C* rv	TTATCGAAACTGACGCTATAAC
pBAD33RBS *phoQ L51C* fw	TACGTTTCGGtgcTTACGTGGCGAG
pBAD33RBS *phoQ L51C* rv	GTTTTATCGAAACTGACG
pBAD33RBS *phoQ L52C* fw	GTTTCGGCTGtgcCGTGGCGAGA
pBAD33RBS *phoQ L52C* rv	GTAGTTTTATCGAAACTGACGC
pBAD33RBS *phoQ R53C* fw	TCGGCTGTTAtgcGGCGAGAGCA
pBAD33RBS *phoQ R53C* rv	AACGTAGTTTTATCGAAACTGACG
pBAD33RBS *phoQ G54C* fw	GCTGTTACGTtgcGAGAGCAATC
pBAD33RBS *phoQ G54C* rv	CGAAACGTAGTTTTATCGAAAC
pBAD33RBS *phoQ E55C* fw	GTTACGTGGCtgcAGCAATCTGTTC
pBAD33RBS *phoQ E55C* rv	AGCCGAAACGTAGTTTTATC
pBAD33RBS *phoQ S56C* fw	ACGTGGCGAGtgcAATCTGTTCT
pBAD33RBS *phoQ S56C* rv	AACAGCCGAAACGTAGTTTTATC
pBAD33RBS *phoQ N57C* fw	TGGCGAGAGCtgcCTGTTCTATACC
pBAD33RBS *phoQ N57C* rv	CGTAACAGCCGAAACGTA
pBAD33RBS *phoQ L58C* fw	CGAGAGCAATtgcTTCTATACCCTTGCGAAGTG
pBAD33RBS *phoQ L58C* rv	CCACGTAACAGCCGAAAC
pBAD33RBS *phoQ F59C* fw	GAGCAATCTGtgcTATACCCTTGCG
pBAD33RBS *phoQ F59C* rv	TCGCCACGTAACAGCCGA
pBAD33RBS *phoQ Y60C* fw	CAATCTGTTCtgcACCCTTGCGAAGTG
pBAD33RBS *phoQ Y60C* rv	CTCTCGCCACGTAACAGC
pBAD33RBS *phoQ T61C* fw	TCTGTTCTATtgcCTTGCGAAGTGGG
pBAD33RBS *phoQ T61C* rv	TTGCTCTCGCCACGTAAC
pBAD33RBS *phoQ L62C* fw	GTTCTATACCtgcGCGAAGTGGGAAAACAATAAG
pBAD33RBS *phoQ L62C* rv	AGATTGCTCTCGCCACGT
pBAD33RBS *phoQ D179C* fw	TGTGGTGGTGtgcACCATTCCGG
pBAD33RBS *phoQ D179C* rv	ATGGTTAATTTTGGCATCC
pBAD33RBS *phoQ T181C* fw	GGTGGATACCtgcCCGGTGGAGC
pBAD33RBS *phoQ T181C* rv	ACCACAATGGTTAATTTTGG
pBAD33RBS *phoQ I183C* fw	TACCATTCCGtgcGAGCTAAAAAGTTCCTATATGG
pBAD33RBS *phoQ I183C* rv	TCCACCACCACAATGGTT

pBAD33RBS *phoQ E184C* fw	CATTCCGGTGtgcCTAAAAAGTTCCTATATG
pBAD33RBS *phoQ E184C* rv	GTATCCACCACCACAATG
pBAD33RBS *phoQ L185C* fw	TCCGGTGGAGtgcAAAAGTTCCTATATG
pBAD33RBS *phoQ L185C* rv	ATGGTATCCACCACCACA
pBAD33RBS *phoQ K186C* fw	GGTGGAGCTAtgcAGTTCCTATATGGTC
pBAD33RBS *phoQ K186C* rv	GGAATGGTATCCACCACC
pBAD33RBS *phoQ S187C* fw	GGAGCTAAAAtgcTCCTATATGGTCTG
pBAD33RBS *phoQ S187C* rv	ACCGGAATGGTATCCACC
pBAD33RBS *phoQ S188C* fw	GCTAAAAAGTtgcTATATGGTCTGG
pBAD33RBS *phoQ S188C* rv	TCCACCGGAATGGTATCC
pBAD33RBS *phoQ S193C* fw	TATGGTCTGGtgcTGGTTTATCTATG
pBAD33RBS *phoQ S193C* rv	TAGGAACTTTTTAGCTCCAC
pBAD33RBS *phoQ W194C* fw	GGTCTGGAGCtgcTTTATCTATG
pBAD33RBS *phoQ W194C* rv	ATATAGGAACTTTTTAGCTCC
pBAD33RBS *phoQ F195C* fw	CTGGAGCTGGtgcATCTATGTGC
pBAD33RBS *phoQ F195C* rv	ACCATATAGGAACTTTTTAGC
pBAD33RBS *phoQ I196C* fw	GAGCTGGTTTtgcTATGTGCTCTC
pBAD33RBS *phoQ I196C* rv	CAGACCATATAGGAACTTTTTAG
pBAD33RBS *phoQ Y197C* fw	CTGGTTTATCtgcGTGCTCTCAG
pBAD33RBS *phoQ Y197C* rv	CTCCAGACCATATAGGAAC
pBAD33RBS *phoQ V198C* fw	GTTTATCTATtgcCTCTCAGCCAATCTGC
pBAD33RBS *phoQ V198C* rv	CAGCTCCAGACCATATAG
pBAD33RBS *phoQ L199C* fw	TATCTATGTGtgcTCAGCCAATCTGC
pBAD33RBS *phoQ L199C* rv	AACCAGCTCCAGACCATA
pBAD33RBS *phoQ S200C* fw	CTATGTGCTCtgcGCCAATCTGC
pBAD33RBS *phoQ S200C* rv	ATAAACCAGCTCCAGACC
pBAD33RBS *phoQ N202C* fw	GCTCTCAGCCtgcCTGCTGTTAG
pBAD33RBS *phoQ N202C* rv	ACATAGATAAACCAGCTC
pBAD33RBS *phoQ L203C* fw	CTCAGCCAATtgcCTGTTAGTGATCCC
pBAD33RBS *phoQ L203C* rv	AGCACATAGATAAACCAG
pBAD33RBS *phoQ L204C* fw	AGCCAATCTGtgcTTAGTGATCCCGC
pBAD33RBS *phoQ L204C* rv	GAGAGCACATAGATAAACC
pBAD33RBS *phoQ L205C* fw	CAATCTGCTGtgcGTGATCCCGC
pBAD33RBS *phoQ L205C* rv	GCTGAGAGCACATAGATAAAC
pBAD33RBS *phoQ V206C* fw	TCTGCTGTTAtgcATCCCGCTGCTGTG
pBAD33RBS *phoQ V206C* rv	TTGGCTGAGAGCACATAG

pBAD33RBS *phoQ I207C* fw	GCTGTTAGTGtgcCCGCTGCTGT
pBAD33RBS *phoQ I207C* rv	AGATTGGCTGAGAGCACATAG
pBAD33RBS *phoQ L209C* fw	AGTGATCCCGtgcCTGTGGGTCG
pBAD33RBS *phoQ L209C* rv	AACAGCAGATTGGCTGAG
pBAD33RBS *phoQ L210C* fw	GATCCCGCTGtgcTGGGTCGCCG
pBAD33RBS *phoQ L210C* rv	ACTAACAGCAGATTGGCTG
pBAD33RBS *phoQ W211C* fw	CCCGCTGCTGtgcGTCGCCGCCT
pBAD33RBS *phoQ W211C* rv	ATCACTAACAGCAGATTGGCTGAGAGCACATAG
pBAD33RBS *phoQ V212C* fw	GCTGCTGTGGtgcGCCGCCTGGT
pBAD33RBS *phoQ V212C* rv	GGGATCACTAACAGCAGATTGGC
pBAD33RBS *phoQ A213C* fw	GCTGTGGGTCtgcGCCTGGTGGA
pBAD33RBS *phoQ A213C* rv	AGCGGGATCACTAACAGC
pTrc99A *mgrB C16A*	GGTGTTGGCTgcgTTGCTGCTTTGGG
pTrc99A *mgrB C16A*	ACGACAACCAGAACGACC
pTrc99A *mgrB C16A W20C* fw	GTTGCTGCTTtgcGCGCAGGTATTC
pTrc99A *mgrB C16A W20C* rv	GCAGCCAACACCACGACA
pTrc99A *mgrB C16A Q22C* fw	GCTTTGGGCGtgcGTATTCAACATGATGTGCG
pTrc99A *mgrB C16A Q22C* rv	AGCAACGCAGCCAACACC
pTrc99A *mgrB C16A F24C* fw	GGCGCAGGTAtgcAACATGATGTG
pTrc99A *mgrB C16A F24C* rv	CAAAGCAGCAACGCAGCC
pTrc99A *mgrB D31C*	GTGCGATCAGtgcGTACAATTTTTCAGC
pTrc99A *mgrB D31C*	ATCATGTTGAATACCTGC
pBAD33RBS *mgrB W20A*	CTTGCTGCTTgcgGCGCAGGTATTC
pBAD33RBS *mgrB W20A*	CAAGCCAACACCACGACA
pBAD33RBS *mgrB C28A*	CAACATGATGgcgGATCAGGATGTACAATTTTTCAGC
pBAD33RBS *mgrB C28A*	AATACCTGCGCCCAAAGC
pET-Duet-1 *mgrB N25-TAG* fw	GCAGGTATTCtagATGATGTGCGATCAG
pET-Duet-1 *mgrB N25-TAG* rv	GCCCAAAGCAGCAAGCAA
pET-Duet-1 *mgrB M26-TAG* fw	GGTATTCAACtagATGTGCGATCAGGATGTACAATTTTTC
pET-Duet-1 *mgrB M26-TAG* rv	TGCGCCCAAAGCAGCAAG
pET-Duet-1 *mgrB M27-TAG* fw	ATTCAACATGtagTGCGATCAGGATGTACAATTTTTCAGCG
pET-Duet-1 *mgrB M27-TAG* rv	ACCTGCGCCCAAAGCAGC
pET-Duet-1 *mgrB D29-TAG* fw	CATGATGTGCtagCAGGATGTACAATTTTTC
pET-Duet-1 *mgrB D29-TAG* rv	TTGAATACCTGCGCCCAA
pET-Duet-1 *mgrB Q30-TAG* fw	GATGTGCGATtagGATGTACAATTTTTC
pET-Duet-1 *mgrB Q30-TAG* rv	ATGTTGAATACCTGCGCC
pET-Duet-1 *mgrB D31-TAG* fw	GTGCGATCAGtagGTACAATTTTTC
pET-Duet-1 *mgrB D31-TAG* rv	ATCATGTTGAATACCTGC
pET-Duet-1 *mgrB V32-TAG* fw	CGATCAGGATtagCAATTTTTCAGCGGAATTTG
pET-Duet-1 *mgrB V32-TAG* rv	CACATCATGTTGAATACCTG
pET-Duet-1 *mgrB Q33-TAG* fw	TCAGGATGTAtagTTTTTCAGCG

pET-Duet-1 *mgrB Q33-TAG* rv	TCGCACATCATGTTGAATAC
pET-Duet-1 *mgrB F34-TAG* fw	GGATGTACAAtagTTCAGCGGAATTTG
pET-Duet-1 *mgrB F34-TAG* rv	TGATCGCACATCATGTTG
pET-Duet-1 *mgrB F35-TAG* fw	TGTACAATTTtagAGCGGAATTTGTG
pET-Duet-1 *mgrB F35-TAG* rv	TCCTGATCGCACATCATG
pET-Duet-1 *mgrB S36-TAG* fw	ACAATTTTTCtagGGAATTTGTGCCATTAACCAG
pET-Duet-1 *mgrB S36-TAG* rv	ACATCCTGATCGCACATC
pET-Duet-1 *mgrB G37-TAG* fw	ATTTTTCAGCtagATTTGTGCCATTAACC
pET-Duet-1 *mgrB G37-TAG* rv	TGTACATCCTGATCGCAC
pET-Duet-1 *mgrB I38-TAG* fw	TTTCAGCGGAtagTGTGCCATTAACC
pET-Duet-1 *mgrB I38-TAG* rv	AATTGTACATCCTGATCG
pET-Duet-1 *mgrB A40-TAG* fw	CGGAATTTGTtagATTAACCAGTTTATC
pET-Duet-1 *mgrB A40-TAG* rv	CTGAAAAATTGTACATCCTG
pET-Duet-1 *mgrB I41-TAG* fw	AATTTGTGCCtagAACCAGTTTATCC
pET-Duet-1 *mgrB I41-TAG* rv	CCGCTGAAAAATTGTACATC
pET-Duet-1 *mgrB N42-TAG* fw	TTGTGCCATTtagCAGTTTATCC
pET-Duet-1 *mgrB N42-TAG* rv	ATTCCGCTGAAAAATTGTAC
pET-Duet-1 *mgrB Q43-TAG* fw	TGCCATTAACtagTTTATCCCGTG
pET-Duet-1 *mgrB Q43-TAG* rv	CAAATTCCGCTGAAAAATTGTAC
pET-Duet-1 *mgrB F44-TAG* fw	CATTAACCAGtagATCCCGTGGTG
pET-Duet-1 *mgrB F44-TAG* rv	GCACAAATTCCGCTGAAAAATTG
pET-Duet-1 *mgrB I45-TAG* fw	TAACCAGTTTtagCCGTGGTGACTG
pET-Duet-1 *mgrB I45-TAG* rv	ATGGCACAAATTCCGCTG
pET-Duet-1 *mgrB P46-TAG* fw	CCAGTTTATCtagTGGTGACTGC
pET-Duet-1 *mgrB P46-TAG* rv	TTAATGGCACAAATTCCG
pET-Duet-1 *mgrB W47-TAG* fw	GTTTATCCCGtagTGACTGCAGG
pET-Duet-1 *mgrB W47-TAG* rv	TGGTTAATGGCACAAATTCC
Nde1 *flag-mgrB* fw	aaaCATATGGATTATAAAGATGATGATGATAAAGGTATGGTGA GCAAGGGCGAGGAG
EcoRV *flag-mgrB* rv	aaaGATATCTCACCACGGGATAAACTG
Nco1 *phoQ(his)$_6$* fw	aaaCCATGGGCAAAAAATTACTGCGTCTTTTTTTCCCGC
BamH1 *phoQ(his)$_6$* rv	aaaGGATCCTTAATGGTGATGGTGATGGTGGC

1034
1035
1036
1037 **SI References**
1038

1039 1. Yadavalli, S.S., et al., *Functional determinants of a small protein controlling a*
1040 *broadly conserved bacterial sensor kinase.* J Bacteriol, 2020.
1041 2. Yuan, J., et al., *Osmosensing by the bacterial PhoQ/PhoP two-component system.*
1042 Proc Natl Acad Sci U S A, 2017. **114**(50): p. E10792-E10798.